TU Delft

Delft University of Technology

Computational investigation of scour around submerged square piles in wave-current flows

Kumar, Lalit; Saud Afzal, Mohammad; Alhaddad, Said

DOI
10.1016/j.oceaneng.2024.119766

Publication date
2024

Document Version
Final published version

Published in
Ocean Engineering

Citation (APA)
Kumar, L., Saud Afzal, M., & Alhaddad, S. (2024). Computational investigation of scour around submerged square piles in wave-current flows. *Ocean Engineering*, *314*, Article 119766. https://doi.org/10.1016/j.oceaneng.2024.119766

Important note
To cite this publication, please use the final published version (if applicable).
Please check the document version above.

Copyright
Other than for strictly personal use, it is not permitted to download, forward or distribute the text or part of it, without the consent of the author(s) and/or copyright holder(s), unless the work is under an open content license such as Creative Commons.

Takedown policy
Please contact us and provide details if you believe this document breaches copyrights.
We will remove access to the work immediately and investigate your claim.

This work is downloaded from Delft University of Technology.
For technical reasons the number of authors shown on this cover page is limited to a maximum of 10.

Ocean Engineering 314 (2024) 119766

Contents lists available at ScienceDirect

Ocean Engineering

journal homepage: www.elsevier.com/locate/oceaneng

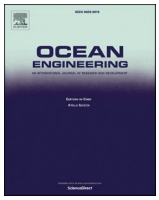

Research paper

Computational investigation of scour around submerged square piles in wave-current flows

Lalit Kumar [a], Mohammad Saud Afzal [a], Said Alhaddad [b,*]

[a] Department of Civil Engineering, Indian Institute of Technology Kharagpur, India
[b] Section of Offshore and Dredging Engineering, Faculty of Mechanical Engineering, Delft University of Technology, Delft, the Netherlands

ARTICLE INFO

Keywords:
Scour
Submergence ratio
Horseshoe vortex
Trailing vortex
Combined wave–current flows

ABSTRACT

This study explores the scour phenomenon around a submerged square pile under the combined influence of waves and currents. To this end, a three-dimensional Computational Fluid Dynamics model was developed. The numerical model solves the Reynolds-averaged Navier-Stokes (RANS) equations with k-ω turbulence closure model. The Level-Set method is utilized to monitor free surface interface realistically within the computational model. The Exner formulation is used to compute the bed elevation variations. An extensive validation is conducted for square pile scour in steady current, wave only, and wave–current conditions. Subsequently, the validated numerical model is utilized to analyze the impact of the submergence ratio, wave-current parameter (U_{cw}), and Keulegan–Carpenter (KC) number on the normalized scour depth around the submerged square pile in combined wave-current flows. The numerical results show that an increase in submergence ratio leads to an increased normalized scour depth around submerged piles in wave-current flows. Furthermore, it was found that a larger U_{cw} results in a larger normalized scour depth around the submerged square pile. However, for larger KC values of 12 and 18, the effect of U_{cw} becomes negligible due to the suppression of lee-wake vortices by developed trailing vortices.

1. Introduction

Submerged piles play a crucial role in coastal environments, serving diverse purposes in infrastructure development, marine construction, and environmental management. These piles are widely utilized as components in pile-like structures, including bridge piers, submerged pile breakwaters, and subsea caissons within coastal environments (Yao et al., 2018). The introduction of submerged piles in coastal areas adds complexity to hydrodynamics and sediment transport phenomena, leading to the formation of scour holes around the piles. The presence of waves and currents simultaneously in coastal environments renders the local scour phenomenon much more complex. Understanding scour is imperative since excessive scouring could cause geotechnical instabilities, such as a breaching flow slide—a dilative failure that occurs when a slope steeper than the sediment internal friction angle is created (Alhaddad et al., 2020, 2023, 2024). Generally, square piles are preferred over circular piles in coastal environments due to their cost-effectiveness and capacity to handle higher moments (Pedram, 2015). Most of the prior investigations concentrated on scouring around circular piles in a steady current. However, limited research has been conducted addressing submerged square pile scour in wave-current conditions.

The introduction of submerged piles with limited heights in the wave-current flows maintains certain key flow features similar to those observed around unsubmerged piles. These features include the downflow and horseshoe vortex (HSV) upstream of the pile, followed by the lee-wake vortices downstream, and an additional trailing vortex emerging above the cylinder. The trailing vortex surpasses the pile, engaging with the lee-wake vortices and ultimately causing the complete suppression of vortex shedding downstream of the pile. Additionally, the diminished height of the pile contributes to a decreased interference with the flow, resulting in a reduction in the intensity of the downflow at the upstream side of the pile. Consequently, this reduction leads to a decrease in the HSV's strength and size. The pictorial representation of the flow structures around the submerged square pile is shown in Fig. 1.

In coastal and marine environments, waves exert a more dominant influence compared to currents. According to Soulsby (1997), the wave-current interaction causes (1) a modification of the phase speed and wavelength of the wave, which causes refraction of waves, (2) bed

* Corresponding author.
E-mail address: S.M.S.Alhaddad@tudelft.nl (S. Alhaddad).

https://doi.org/10.1016/j.oceaneng.2024.119766
Received 5 June 2024; Received in revised form 7 November 2024; Accepted 9 November 2024
Available online 15 November 2024
0029-8018/© 2024 The Authors. Published by Elsevier Ltd. This is an open access article under the CC BY-NC-ND license (http://creativecommons.org/licenses/by-nc-nd/4.0/).

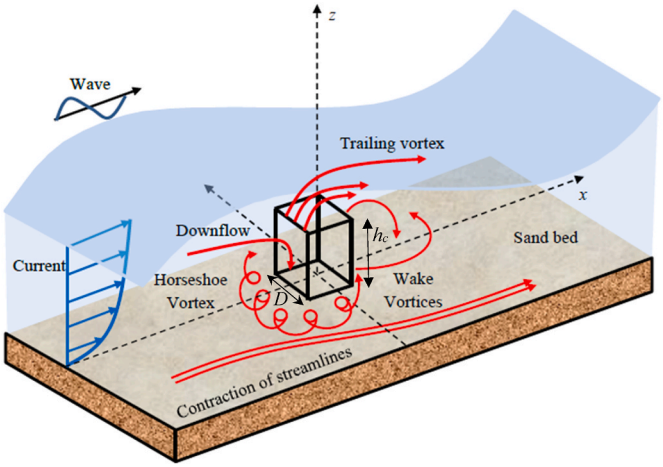

Fig. 1. Three-dimensional representation of flow pattern around a submerged square pile.

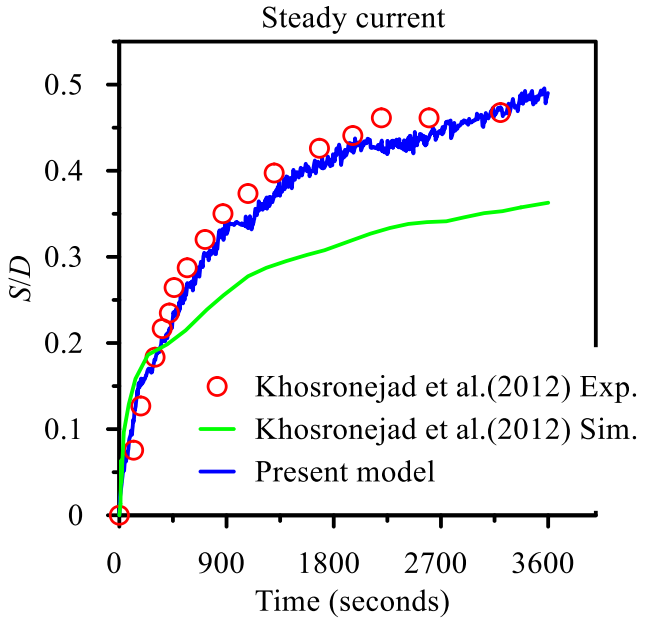

Fig. 2. Numerical model validation with experimental findings of Khosronejad et al. (2022) for square pile scour under steady currents.

shear stress increment due to wave-current boundary layer interactions, and (3) the development of wave-generated currents. In combined wave-current flows, the Keulegan-Carpenter (KC) number and wave-current parameter (U_{cw}) governed the pile scour phenomenon (Sumer and Fredsøe, 2001). The KC and U_{cw} parameters can be expressed as given in Eqs. (1) and (2).

$$KC = \frac{U_w T}{D} \tag{1}$$

$$U_{cw} = \frac{U_c}{U_c + U_w} \tag{2}$$

where U_w is the wave's orbital velocity of the water particle near the sediment bed in undisturbed condition, U_c is the velocity of the steady current in undisturbed condition, D is the square pile width obstructing the flow in the y direction, and T is the wave period.

In combined wave-current flow, Qi and Gao (2014b) performed an experimental study on pile scour and proposed a non-dimensional

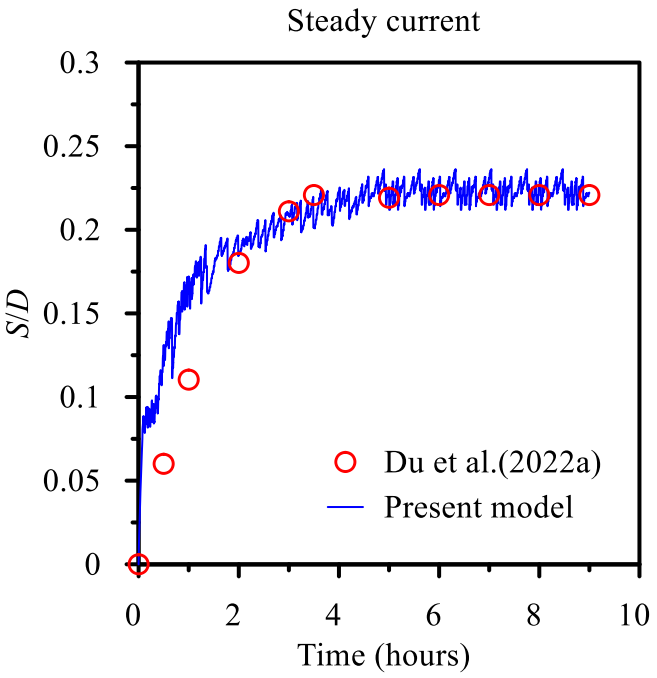

Fig. 3. Numerical model validation with experimental findings of Du et al. (2022a) for submerged square pile scour under steady currents.

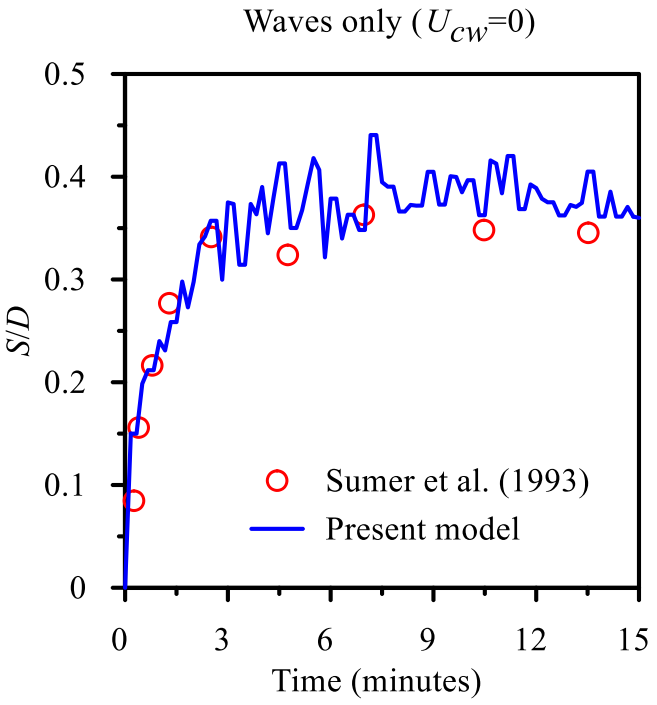

Fig. 4. Numerical model validation with experimental results of Sumer et al. (1993) for square pile scour under wave-only.

parameter known as the average-velocity based Froude number (Fr_a). The Fr_a can be represented as provided in Eq. (3).

$$Fr_a = \frac{U_a}{\sqrt{gD}} \tag{3}$$

where U_a is the average water particle velocity during one-quarter cycle of oscillation in combined wave-current flows, and can be represented as

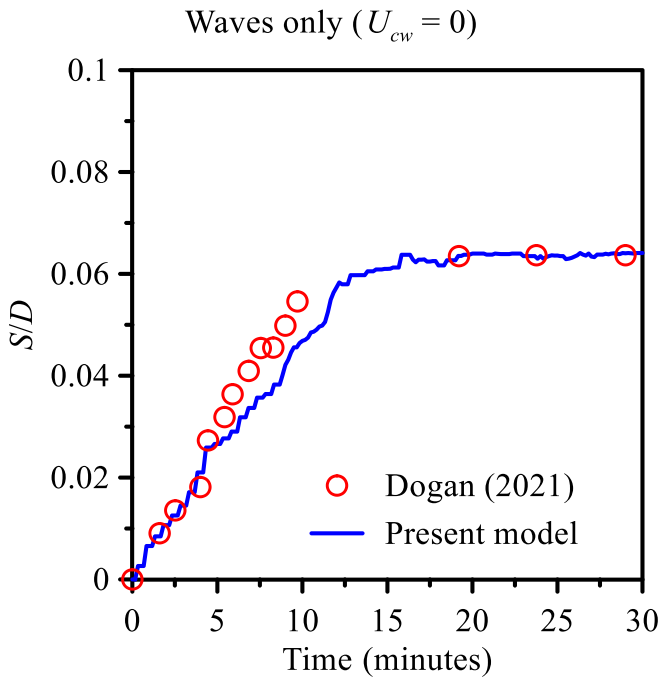

Fig. 5. Numerical model validation with experimental findings of Dogan (2021) for circular pile scour under wave-only.

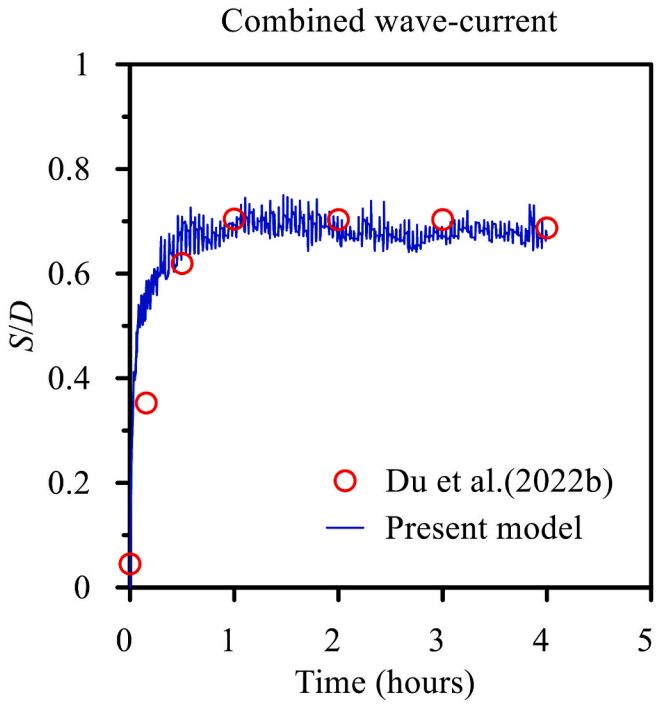

Fig. 6. Numerical model validation with experimental results of Du et al. (2022b) for the temporal variation of the submerged square pile in wave-current flows.

given in Eq. (4).

$$U_a = \frac{1}{T/4}\int_0^{T/4} (U_c + U_w \sin(2\pi t / T))dt = U_c + \frac{2}{\pi}U_w \quad (4)$$

Most studies on local scour around a submerged cylinder are

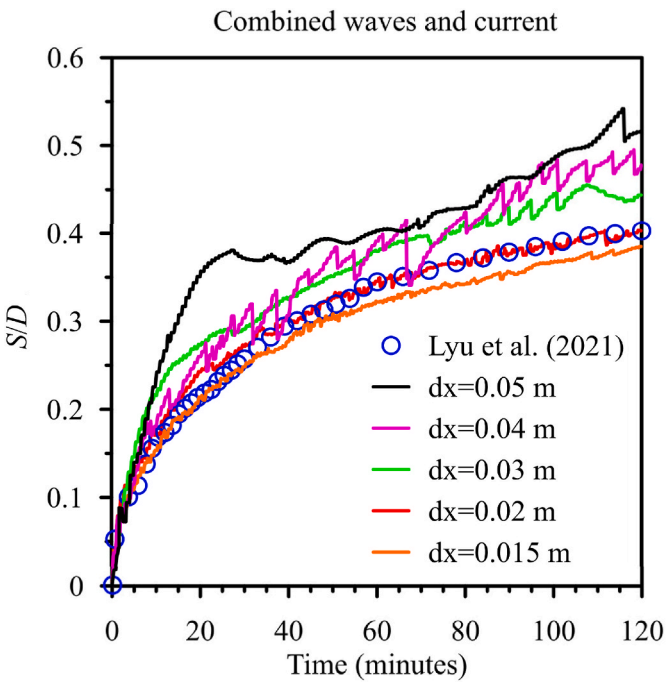

Fig. 7. Numerical model validation with grid convergence against experimental results of Lyu et al. (2021) for the temporal variation of circular pile scour in wave-current flow.

conducted under steady flows (Dey et al., 2008; Du et al., 2022a; Yao et al., 2018; Zhao et al., 2010). In one of the notable studies, Dey et al. (2008) conducted an experimental investigation on scour around a submerged vertical circular cylinder under a steady current. They compared results between unsubmerged and submerged cylinders under identical flow conditions, finding that an increase in submergence ratio (flow depth to pile height) led to decreased scour depth in a steady current. Further, Zhao et al. (2010) examined the submerged circular pile scour under steady flow conditions. The numerical findings were verified by comparing them with the experimental results. They varied the cylinder height-to-diameter ratios (h_c/D, where h_c is the height of the square pile above the bed level) with a constant flow depth, observing a decrease in scour depth as the cylinder height decreased. In the case of short cylinders with $h_c/D \leq 0.5$, the lack of vortex shedding resulted in the absence of scour beneath the cylinder. Conversely, for h_c/D ratios exceeding 2, the scour depth demonstrated almost no dependency on h_c. Further, Yao et al. (2018) examined the scour at submerged square (45° and 90° orientation) and circular cylinder piles in steady currents. Their study focused on local scour with h_c/D ranging from 0.1 to 8, considering clear water and sheet flow conditions. They reported decreased equilibrium scour depth (S) for $h_c/D \leq 4$.

Several notable works have been conducted to explore the scour phenomena around non-submerged circular piles, particularly in wave-current flows (Chen and Li, 2018; Eadie IV and Herbich, 1987; Qi and Gao, 2014a; Qi and Gao, 2014b; Sumer and Fredsøe, 2001). However, few studies have specifically examined the submerged pile scour in wave-current flows (Du et al., 2022b; Lyu et al., 2021). Lyu et al. (2021) performed an experimental investigation on local scour around submerged circular piles in combined wave-current. They reported that the HSV and vortex shedding phenomenon weaken when the monopile height or submergence ratio (h_c/D) decreases. They also examined the effect of *KC* and Froude numbers (*Fr*) on pile scour in wave-current flows. Recently, Du et al. (2022b) performed an experimental study to examine submerged square pile scour in wave-current flows. They observed that the pile height-to-width ratio significantly affects the equilibrium scour depth. However, the scope of their experimental study is confined to lower *KC* regimes and a limited range of wave-current

parameters (U_{cw}).

Recently, several researchers have performed experimental and numerical studies on sediment transport phenomena. Khosronejad et al. (2020) performed an experimental and numerical study on sediment transport around an abutment using rigid-lid (*RL*) and level-set methods (LSM), respectively, for large eddy simulations (LES). Their numerical model shows good agreement with the experimental results. Similarly, Sogut et al. (2022) performed laboratory experiments and numerical simulations using the Monte Carlo method to examine scour around a square structure on a sandy berm. Their three-dimensional (3D) Eulerian two-phase model, SedWaveFoam, agrees with the experimental results of non-equilibrium scour around sharp-edged square structures for low KC numbers. Further, Lancaster et al. (2022) performed a comprehensive numerical study on wave-induced scour around a bluff body. The numerical model REEF3D was tested in various wave conditions, structure geometries, and sediment sizes to accurately estimate scour. Their findings indicate that the non-dimensional scour depth does not vary significantly with the sediment size or structure dimensions. Recently, Velioglu Sogut et al. (2024) performed a numerical study to examine non-equilibrium scour depth at emerged structure under transient wave. They have used the SedWaveFoam and FLOW3D models to estimate vortex-induced velocities and bed evolution. The results indicated that the bed evolution is better predicted using the FLOW3D numerical model.

Based on the literature discussed above, it can be observed that experimental approaches are often favored to examine the scour phenomenon around the submerged pile due to their ability to replicate real-world circumstances closely. However, numerical modelling can provide an accurate and cost-effective means to supplement experimental studies. Therefore, the main objective of the present research is to examine the normalized equilibrium scour depth (S/D) around submerged square piles in wave-current flows with varying *KC,* $U_{cw,}$ and h_c/D parameters. This work is the first to examine scour processes around submerged square piles in wave-current flows using a three-dimensional semi-coupled model. A semi-coupled model solves the flow hydrodynamics and sediment transport separately, as detailed in the following section.

2. Numerical model

The scour around the submerged square pile was examined using a unique three-dimensional numerical model that includes wave-current flows. This study utilizes the open-source computational fluid Dynamics (CFD) model REEF3D to simulate submerged pile scour in wave-current flows. The present model is a three-phase, semi-coupled model with great potential for capturing the free surface interface. The REEF3D algorithm solves the continuity equation and the incompressible Reynolds-averaged Navier-Stokes (RANS) equations to determine the pressure and velocity terms. The continuity and RANS equations are given in Eqs. (5) and (6).

$$\frac{\partial U_i}{\partial x_i} = 0 \tag{5}$$

$$\frac{\partial U_i}{\partial t} + U_j\frac{\partial U_i}{\partial x_j} = -\frac{1}{\rho}\frac{\partial P}{\partial x_i} + \frac{\partial}{\partial x_j}\left[(\upsilon + \upsilon_t)\left(\frac{\partial U_i}{\partial x_j} + \frac{\partial U_j}{\partial x_i}\right)\right] + g_i \tag{6}$$

where U denotes the ensemble average velocity over time t. P is the pressure, g is the gravitational acceleration, which is a specific case of volumetric forces, ν denotes the kinematic viscosity and ν_t denotes the turbulent eddy viscosity, respectively.

The present investigation employs the k-ω turbulence model (Wilcox, 1994) to capture the turbulence flow hydrodynamics. The k-ω turbulence method resolves the partial differential equations involving two variables: the turbulent kinetic energy (k) and the turbulent dissipation (ω), which establishes the turbulence's scale. Using k and ω, one can determine the turbulent eddy viscosity (ν_t). The turbulent kinetic energy (k) and specific turbulent dissipation (ω) formulation are given in Eqs. (7) and (8).

$$\frac{\partial k}{\partial t} + u_j\frac{\partial k}{\partial x_j} = \frac{\partial}{\partial x_j}\left[\left(\nu + \frac{\nu_t}{\sigma_k}\right)\frac{\partial k}{\partial x_j}\right] + P_k - \beta_k k\omega \tag{7}$$

$$\frac{\partial \omega}{\partial t} + u_j\frac{\partial \omega}{\partial x_j} = \frac{\partial}{\partial x_j}\left[\left(\nu + \frac{\nu_t}{\sigma_\omega}\right)\frac{\partial \omega}{\partial x_j}\right] + \frac{\omega}{k}\alpha P_k - \beta\omega^2 \tag{8}$$

where $\alpha = 5/9$, $\beta = 3/40$, $\beta_k = 9/100$, $\sigma_k = 2$, and $\sigma_\omega = 2$ are the coefficients, and the turbulent production rate (P_k) can be calculated using Eq. (9).

$$P_k = \nu_t\frac{\partial u_i}{\partial x_j}\left[\frac{\partial u_i}{\partial x_j} + \frac{\partial u_j}{\partial x_i}\right] \tag{9}$$

The equation takes into consideration the limited value of the eddy viscosity ν_t. It prevents excessive turbulence formation in flow that is too stressed outside of the boundary layer (Durbin, 2009). As a result, the hydrodynamic model's minimal eddy viscosity value is determined using Eq. (10).

$$\nu_t = \min\left(\frac{k}{w}, \sqrt{\frac{2}{3}}\frac{k}{S_s}\right) \tag{10}$$

Further, the numerical error in the formulation may result from overproduction of magnitude of shear strain (S_s) at the water-air interface, which would create unrealistically high turbulence across the interface, even if damping is unavoidable in wave-current flows. To address this challenge, the formulation proposed by Naot and Rodi (1982) is utilized in the numerical model.

The projection model (Chorin, 1968) is utilized to model the pressure gradient in the RANS equation. This model necessitates an explicit time treatment of the RANS equation in the case of incompressible flow. The Fully Parallelized Jacobi-Preconditioned BiCGStab solver (Van Der Vorst, 1992) is employed for solving the Poisson equation. The convective term U_i of the RANS equation is discretized within a conservative finite difference method using the 5th-order Weighted Essentially Non-Oscillatory (WENO) scheme (Jiang and Shu, 1996). To improve temporal accuracy, the 3rd order Total Variation Diminishing (TVD) Runge-Kutta scheme (Shu and Gottlieb, 1998) is employed for time discretization. The TVD features implemented adaptive time stepping to ensure numerical stability for Courant-Friedrichs-Lewy (CFL) numbers less than 1. In CFD modelling, the Courant-Friedrichs-Lewy (CFL) condition is a stability criterion used for solving the partial differential equations, especially for problems involving advection and wave propagation. It can be represented as given in Eq. (11).

$$CFL = \frac{u\Delta t}{\Delta x} < 1 \tag{11}$$

where u is the characteristic velocity of the flow, Δt is the time step size, and Δx is the spatial grid size.

In combined wave-current flow, both wave and current components contribute to the overall flow velocity. Therefore, the CFL criterion ensures that the numerical time step is small enough to accurately resolve both the wave-induced and current-induced motions without causing numerical instabilities. In the present study, the CFL criterion was fixed equal to 0.1 to maintain numerical stability while capturing the complex wave-current interactions and critical flow features such as vortex shedding, scour development, and flow separation, which are important for accurately predicting the scour depth around the submerged pile. This balance between numerical accuracy and computational efficiency was crucial for obtaining reliable numerical results.

The present numerical model utilizes the Level set method (LSM) developed by Osher and Sethian (1988) to compute the free surface realistically and analyze the two-phase interface motion in three

dimensions. The LSM is employed to simulate the sediment-water and water-air interface. The smooth signed distance function utilizes a zero-level set to depict the bed surface's evolution accurately. The level set function provides the closest distance to the interface at each position. However, different signs are used to demonstrate the distinct model's phases. The LSM has the advantage of eliminating numerical instability and differentiating fluid interface. The REEF3D code employs a ghost cell immersed boundary approach for dealing with complex geometry on a Cartesian grid. The ghost cell is a specific type of immersed boundary approach capable of treating arbitrary submerged bodies on cartesian grids (Mingham and Causon, 2000). The immersed boundary is regarded as a sharp interface in the ghost cell approach. In the governing equation, discrete forces are explicitly excluded. It explicitly excludes the discrete forces from the governing equation.

Consequently, its integration with the existing solver is complicated. The REEF3D code decomposes the numerical domain through the utilization of parallel processing. To facilitate communication across distinct domains, the ghost cell technique is implemented, with each domain being subdivided into smaller domains.

2.1. Sediment transport modeling

Sediment transport is highly influenced by the bed shear stress, which can be calculated using turbulent viscosity. The bed shear stress formulation is essential for predicting the sediment transport by determining the initiation and rates of sediment movement (Dutta et al., 2023). Therefore, Dey (2014) formulation was used to calculate bed shear stress with turbulent viscosity, given in Eq. (12).

$$\tau = -\rho(\upsilon_t + \upsilon)\frac{\partial U}{\partial z} \tag{12}$$

Engelund and Fredsoe (1976) formulation is utilized to calculate bedload sediment transport rates, as shown in Eq. (13).

$$\begin{aligned} q^*_{b,i} &= 0;\ \tau^* < \tau^*_{c,i} \\ q^*_{b,i} &= 18.74\left(\tau^* - \tau^*_{c,i}\right)\left(\tau^{*0.5} - 0.7\tau^{*0.5}_{c,i}\right);\ \tau > \tau^*_{c,i} \\ \tau^*_{c,i} &= \frac{\tau_{c,i}}{(\rho_s - \rho)gd_{50}} \end{aligned} \tag{13}$$

where ρ_s is the density of sediment particles, ρ is water density, $q^*_{b\,i}$ is the bed load transport rate, d_{50} is the diameter of the median sediment particle, $\tau^*_{c,i}$ is the non-dimensional critical shear stress and the subscript i refers to the time step iteration in the numerical scheme.

The suspended sediment load transport is calculated using the van Rijn (1984) equation, which is provided in Eq. (14).

$$\frac{\partial c}{\partial t} + U_j\frac{\partial c}{\partial x_j} + w_s\frac{\partial c}{\partial z} = \frac{\partial}{\partial x_j}\left(\Gamma\frac{\partial c}{\partial x_j}\right) \tag{14}$$

Here w_s denotes the terminal fall velocity, c denotes the concentration of suspended load Γ denotes the coefficient of diffusion, which is equal to eddy viscosity. The solution of the convection-diffusion equation is based on the near-bed sediment concentration (c_b) and the free surface's zero vertical sediment flux. The concentration of sediment (c_b) near the bed is calculated using van Rijn (1984) formulation, shown in Eq. (15).

$$c_b = 0.015\frac{d_{50}}{a}\left(\frac{T^{1.5}}{D^{0.3}_*}\right) \tag{15}$$

where a denotes the suspended sediment load reference level, which is equal to equivalent bed roughness, and D^* represents the particle diameter, computed using Eq. (16).

$$D_* = d_{50}\left[\frac{(s-1)g}{\nu^2}\right]^{1/3} \tag{16}$$

In addition, the critical bed shear stress (τ_o) on the horizontal bed slope is determined utilizing the Shields diagram. The topography of the seabed changes into longitudinal and transversely sloping beds when the scour process initiates. As a result, the influence of a sloping bed is a crucial factor in the computation of the reduced critical bed shear stress (τ_c), since it contributes to the sediment incipient motion. Therefore, a reduction factor (r) is introduced to derive the reduced critical shear stress, which is multiplied by the flatbed critical shear stress (τ_o), as specified in Eq. (17).

$$\tau_c = r\,\mathrm{x}\tau_o \tag{17}$$

To determine this reduction factor (r), Dey (2003) analytical formulation is used in the present numerical model, given in Eq. (18).

$$\begin{aligned} r = \frac{1}{(1-\eta\tan\varphi)\tan\varphi}\{ &-\left(\sin\theta + \eta\tan^2\varphi\sqrt{\cos^2\theta - \sin^2\alpha}\right) \\ &+\left[\left(\sin\theta + \eta\tan^2\varphi\sqrt{\cos^2\theta - \sin^2\alpha}\right)^2\right] \end{aligned} \tag{18}$$

where η represents the ratio of the drag force to the inertia force.

The sand-slide technique was utilized to prevent excess sediment transport downstream, as the bed slope becomes greater than the angle of repose (φ) (Burkow and Griebel, 2016). Additionally, a −2% slope adjustment was implemented to further stabilize the sediment bed, as recommended by Roulund et al. (2005). This combination effectively reduces the bed slope gradient, minimizing sediment movement and maintaining sediment stability. A more in-depth discussion of the numerical model can be found in Kumar and Afzal (2023).

2.2. Numerical model setup

The numerical wave tank (NWT) is an economical and time-efficient substitute for physical modeling when examining combined wave-current flows. Waves are produced at the inlet of a confined domain and absorbed at the other extremity in NWT simulations. To maintain accurate wave hydrodynamics and sediment transport, generating waves at the inlet and eliminating wave reflection at the absorption end is critical. Therefore, the relaxation method (Jacobsen et al., 2011) is utilized to generate waves in the present NWT, while the Active Wave Absorption (AWA) method is implemented to mitigate wave reflection. In conjunction with the Dirichlet boundary condition, second-order Stokes waves simulate oscillatory and combined wave-current flows at the NWT inlet. Unlike traditional NWT used for experimental conditions, which necessitate significant resource allocation and time consumption, the present study opts for a truncated or reduced-size NWT that serves as a practical substitute for a full-sized tank, providing accurate and reliable results for scour in coastal environments (Afzal et al., 2020; Gautam et al., 2021).

2.3. Numerical model validation

The present study utilizes the sediment transport module of REEF3D to simulate submerged pile scour in wave-current flow. Nevertheless, it is imperative to validate the numerical model to ensure an accurate estimation of equilibrium scour depth (S) around submerged square piles in various flow scenarios. The validation procedure assesses the model's reliability and performance under these specific conditions. In steady current, the numerical model results were validated against the experimental data of Khosronejad et al. (2012) for an unsubmerged square pile and Du et al. (2022a) for a submerged square pile. In wave-only conditions, the numerical simulation results were validated using the temporal development of scour around a square pile (Sumer et al., 1993) and a circular pile (Dogan, 2021) due to the lack of experimental studies on submerged square pile scour. Further, the validation of the numerical model against experimental data from Du et al. (2022b) was conducted for the scour around submerged square

piles in wave-current flow. In addition, the present study has performed supplementary validation of circular pile scour in wave-current flow against Lyu et al. (2021), along with a grid convergence study. The experimental parameters employed in the numerical simulations for the validation are presented in Table 1.

2.3.1. Steady current

In steady current, Khosronejad et al. (2012) performed an experimental investigation of square pile scour using an edge length of 16.51 cm. The square pier was made from rigid, hydraulically smooth material to minimize surface friction effects. The pier was placed vertically along the centerline of a mobile-bed rectangular flume, measuring 10 m in length, 1.21 m in width, and 45 cm in depth, with a 20 cm deep layer of uniformly graded, non-cohesive fine sand of d_{50} equals to 0.85 mm on the bed. The flow water depth was fixed to 0.139 m with the mean inflow velocity of 0.22 m/s, corresponding to a Reynolds number of 30, 580. The setup maintained clear-water scour conditions with a steady inflow rate and free-flow outlet to avoid backwater effects. Further, they validated their experimental results using the curvilinear immersed boundary (FSI-CURVIB) method. The hydrodynamic model employs a second-order accurate fractional step method to solve the unsteady Reynolds-averaged Navier–Stokes (URANS) equations, coupled with the k-ω turbulence model. The computational domain was discretized using a Cartesian grid with unstructured triangular mesh for accurate representation of the structure and sediment/water interface. The flume boundaries were set to a no-slip condition at the walls, while a free-surface boundary was maintained at the water-air interface to allow a free surface flow. The bed erosion is modeled by solving the sediment continuity equation in the bed-load layer using a second-order accurate unstructured finite-volume formulation, which includes a sand-slide and bed-slope-limiting algorithm. Further, the present numerical model replicates both the experimental setup and flow conditions of Khosronejad et al. (2012) and validates its results with their findings on the temporal variation of square pile scour, as shown in Fig. 2.

The experimental results obtained by Khosronejad et al. (2012) for square pile scour (T = 1 h) are indicated by red discrete points, while the blue line shows the numerical simulation results. The measured equilibrium scour depth (S) in the numerical simulation was 8 cm, which is consistent with the experimental measurement of 7.72 cm. Additionally, the numerical simulation findings by Khosronejad et al. (2012) are compared with the experimental results. The numerical models of Khosronejad et al. (2012) underestimate the results of the temporal variation of scour. However, the present numerical model outperforms Khosronejad et al. (2012) in predicting equilibrium scour depth and exhibits good agreement with the experimental temporal variation of scour at the square pile. The difference between the present simulation and the numerical results of Khosronejad et al. (2012) could be attributed to the estimation of the critical Shields parameter for sediment particle initiation, which was not provided in their study. The absence of this parameter in Khosronejad et al. (2012) numerical simulation results in discrepancies between their simulation and the experimental results (Bordbar et al., 2021). To address this, the present numerical study estimated the critical Shields parameter using the equation proposed by (Soulsby and Whitehouse, 1997) and applied it in the numerical simulations. This approach resulted in a good agreement with the experimental results of Khosronejad et al. (2012).

Based on statistical metrics provided by Şen et al. (2022), the developed numerical model significantly outperforms the Khosronejad et al. (2012) numerical model in predicting the temporal development of scour with steady current. The developed CFD model shows a stronger correlation between predicted and experimental values, with a coefficient of determination (R^2) of 0.983, compared to 0.932 for the Khosronejad et al. (2012) model. It also demonstrates near-perfect agreement, with an index of agreement (Willmott, 1981) of 0.994, compared to 0.86 for the Khosronejad et al. (2012) model. Additionally, the developed CFD model has a much lower root mean square error (RMSE) of 0.022, compared to 0.088 for the Khosronejad et al. (2012) model, indicating higher accuracy. The Nash-Sutcliffe model efficiency coefficient (NSE) for the developed CFD model is 0.976, further highlighting its superior predictive power compared to the Khosronejad et al. (2012) model.

Similarly, the experimental results of Du et al. (2022a) has been utilized to validate the present numerical model. They have performed an experimental study using a submerged square pile in a flume of 60 m long, 1.2 m wide, and 1.5 m deep. A uniform sand bed of depth 0.2m with median sediment size (d_{50}) of 0.65 mm was used. A square pile model of 10 cm width was placed in the centre of the flume. The submergence ratio (h_c/D) was kept fixed to 2. They have kept the flow depth of 0.5 m with a flow velocity of 0.176 m/s. The Froude number and Reynolds number are calculated to be 0.0794 and 88000, respectively. Similarly a reduced size numerical wave tank of dimension 6 m × 1.2 m × 1.5 m is utilized to replicate the flow characteristics in the present study. To validate the present numerical model, the results were compared with the experimental data on the temporal variation of submerged square pile scour from Du et al. (2022a) shown in Fig. 3.

The experimental results obtained by Du et al. (2022a) for submerged square pile scour (T = 9 h) are represented by red discrete circles, while the blue line plot shows the numerical simulation results. The equilibrium scour depth in the numerical simulation was found to be 2.2 cm, which is in good agreement with the 2.17 cm experimental result. Similarly, the numerical results of the temporal variation of the submerged square pile scour pattern closely match the experimental findings of Du et al. (2022a). Based on the statistical performance metrics, the present numerical model shows good agreement with the experimental results of Du et al. (2022a) for the prediction of temporal scour depth around the submerged square pile in a steady current. It has an R^2 value of 0.882, showing a strong correlation between predicted and experimental values. The index of agreement and $RMSE$ were observed 0.955 and 0.029, respectively, which represents better reliability and good accuracy of numerical model. The NSE value of 0.846 highlights the model's strong predictive power in submerged conditions.

2.3.2. Wave only

In wave-only conditions, the numerical simulation results were validated using the temporal development of scour around a square pile (Sumer et al., 1993) and a circular pile (Dogan, 2021) due to the lack of experimental studies on submerged square pile scour. Sumer et al. (1993) performed an experimental study on scour around the square piles in wave-only conditions. They have performed their experiments in a rectangular wave flume of 26.5 m × 0.6 m x 0.8 m. A uniform sand bed

Table 1
Experimental conditions for the validation of the numerical model.

Cases	D (m)	d_{50} (mm)	H (m)	T_w (s)	U_w (m/s)	U_c (m/s)	U_{cw}	KC	S/D
Current-only (Fig. 2) (Khosronejad et al., 2012)	0.16	0.85	–	–	–	0.22	1	–	0.47
Current-only (Fig. 3) (Du et al., 2022a), Run 3	0.1	0.65	–	–	–	0.176	1	–	0.22
Wave only (Fig. 4) (Sumer et al., 1993),Run 9	0.02	0.18	0.14	1.4	0.31	–	0	22	0.35
Wave only (Fig. 5) (Dogan, 2021), Run 44	0.2	1.85	0.2	2.7	0.375	–	0	5.1	0.06
Wave-current (Fig. 6) (Du et al., 2022b), Run 2	0.1	0.18	0.11	1.6	0.178	0.221	0.55	2.9	0.68
Wave-current (Fig. 7) (Lyu et al., 2021), Run 3	0.16	0.22	0.09	1	0.131	0.22	0.63	0.8	0.40

of 0.2 m depth with median sediment size (d_{50}) of 0.18 mm was used. A square pile model of 20 mm width was placed in the centre of the flume. The flow water depth was maintained constant at 40 cm, and the wave orbital velocity was considered 0.31 m/s. In their experiments, the wave period and wave height were 1.4 s and 10 cm, respectively. The Froude number and Reynolds number are calculated to be 0.156 and 12400, respectively. Similarly, a reduced size numerical wave tank (6 m × 0.6 m × 0.8 m) is utilized to replicate the flow characteristics in the present study. To validate the present numerical model, the results were compared with the experimental data on the temporal variation of submerged square pile scour from Sumer et al. (1993), shown in Fig. 4.

In the numerical simulation, the observed equilibrium scour depth was 8 mm, closely aligning with the experimental observation of 7 mm. Similarly, the numerical results of the temporal development of the square pile scour pattern closely match the experimental findings reported by Sumer et al. (1993). Based on the statistical comparison metrics, the developed numerical model has a moderate performance in predicting the temporal development of scour in wave-only conditions. The numerical model shows a R^2 value of 0.753, which indicates a reasonable correlation between the predicted and experimental values of Sumer et al. (1993). Further, the index of agreement and *RMSE* were 0.909 and 0.062, respectively, which shows good reliability and a higher average deviation from the experimental values. The *NSE* is 0.554, indicating moderate predictive power. The developed numerical model shows fairly accurate results in predicting temporal scour depth.

Further, the experimental results of Dogan (2021) have been utilized to validate the present numerical model in wave-only conditions. Dogan (2021) performed an experimental study on wave-induced scour around a large pile. Dogan (2021) utilized a rectangular wave channel of 33 m × 3.6 m × 1.2 m to conduct scour experiments. A uniform sand bed of 0.17 m depth with median sediment size (d_{50}) of 1.85 mm was used. A circular pile model of 20 cm diameter was placed in the centre of the flume. The flow water depth was maintained constant at 55 cm, and the wave orbital velocity was considered 0.375 m/s. The waves are generated with a wave period of 2.7 s and a wave height of 20 cm. The wave induced Froude number and Reynolds number are calculated to be 0.161 and 20,625, respectively. Similarly, a reduced size numerical wave tank (6 m × 3.6 m × 1.2 m) is utilized to replicate the flow characteristics in the present study. To validate the present numerical model, the results were compared with the experimental data on the temporal variation of submerged square pile scour from Dogan (2021), shown in Fig. 5.

The numerical simulations were performed for only 30 min, as the experimental findings indicated that the scour reached equilibrium within this time frame, thereby reducing the computational cost. In numerical simulation, the observed equilibrium scour depth was 12.8 mm, which is in good agreement with the experimental observation of 12.7 mm. The present model results of the temporal variation of the square pile scour pattern closely matched the experimental observations of Dogan (2021). However, a slight temporal variation is evident in the numerical results, indicating discernible patterns of erosion and deposition. The present developed model shows excellent performance in predicting the temporal development of scour in wave-only conditions for a circular pile. It has a very high R^2 value of 0.963, indicating a strong correlation between predicted and experimental data of Dogan (2021). The numerical model predicts temporal development of scour with index of agreement value of 0.984, which represents almost perfect agreement. The *RMSE* was observed very low at 0.005, which suggests that the model's predictions are extremely accurate. Further, the *NSE* is 0.938, highlighting its strong predictive power. These metrics collectively indicate that the developed model is highly reliable and accurate for modeling scour development in these conditions.

2.3.3. Combined waves and current flow

In combined wave-current conditions, the numerical simulation results were validated using the temporal development of scour around a submerged square pile (Du et al., 2022b) and a circular pile (Lyu et al., 2021). Du et al. (2022b) performed an experimental study on scour around the submerged square piles in combined wave-current conditions. They have performed an experimental study using a submerged square pile in a flume of 60 m × 1.2 m x 1.5 m. A uniform sand bed of 0.2 m depth with median sediment size (d_{50}) of 0.18 mm was used. A square pile model of 0.1 m diameter was placed in the centre of the flume. The submergence ratio (h_c/D) was kept fixed, equal to 1. The flow water depth was maintained constant at 50 cm, and the current velocity was considered 0.221 m/s. In their experiment, the wave period was 1.6 s, and the wave height was 0.11 m. The Froude number and Reynolds number are calculated to be 0.080 and 89000, respectively. Similarly, a reduced size numerical wave tank (6 m × 1.2 m x 1.5 m) is utilized to replicate the flow characteristics in the present study. To validate the present numerical model, the results were compared with the experimental data on the temporal variation of submerged square pile scour from Du et al. (2022b), shown in Fig. 6. The measured equilibrium scour depth in the numerical simulation was 6.71 cm, which was in good agreement with the 6.8 cm experimental result. The numerical results for temporal variation of the submerged square pile scour pattern closely align with the experimental findings of Du et al. (2022b) during the initial and equilibrium phases. However, a slight over prediction is noticeable in the numerical results during the initial phase of scour.

The presently developed CFD model shows excellent performance in predicting the temporal development of scour around a submerged square pile in combined wave-current flow. The developed numerical model's predicts temporal development of scour with a R^2 value of 0.956, which indicates a very strong correlation between the predicted and experimental data of Du et al. (2022b). The model shows an index of agreement of 0.987, which represents the model's predictions align perfectly with the experimental findings. The *RMSE* was found 0.056, which is quite low, suggesting that the model's predictions are very accurate. Further, the high *NSE* value of 0.944 reflects the model's ability to accurately reproduce the observed scour development.

Further, the experimental results of Lyu et al. (2021) have been utilized to validate the present numerical model for pile scour in combined wave-current flow. They have performed an experimental study using emergent circular monopile in a flume of 45 m × 0.8 m x 1.0 m. A uniform sand bed of 0.6 m depth with median sediment size (d_{50}) of 0.22 mm was used. A circular monopile model of 0.16 m diameter was placed in the centre of the flume. The flow water depth was maintained constant at 0.4 m, and the current velocity was considered 0.22 m/s. In their experiments, the wave period and wave height were 1 s and 9 cm, respectively. The Froude number and Reynolds number are calculated to be 0.111 and 88000, respectively. Similarly, a reduced size numerical wave tank of 6 m × 0.8 m x 1.0 m is utilized to replicate the flow characteristics of Lyu et al. (2021) in the present study. The numerical model findings of pile scour with the experimental results of Lyu et al. (2021) are shown in Fig. 7. Further, a comprehensive grid convergence study has been conducted to evaluate how the size of the computational grid impacts the accuracy and reliability of numerical simulations. This analysis is important to ensure the accuracy and robustness of the numerical results.

A grid convergence study was carried out using various uniform grid sizes in all the directions of 5, 4, 3, 2, and 1.5 cm. The coarser grids of 5 cm and 4 cm exhibited significant deviations from the experimental data. A grid convergence study was carried out using various uniform grid sizes (dx) of 5, 4, 3, 2, and 1.5 cm. The coarser grids of 5 cm and 4 cm exhibited significant deviations from the experimental data. However, when the grid size was reduced to 3 cm, the model's performance showed marked improvement, and a further reduction to 2 cm brought the results into even closer alignment with the experimental findings of Lyu et al. (2021). A finer grid size of 1.5 cm shows slight lesser values of temporal development of scour in comparison to observed values, which may be due to numerical instabilities that occurs when the time step is not sufficiently reduced, leading to incorrect results or failed

convergence. In a numerical computation round-off errors are also introduced at every stage of computation. These round-off errors become more pronounced with smaller grid sizes as the finite precision of computer arithmetic accumulates, diminishing result accuracy. It can be observed that the reduction in grid size from the optimum level does not significantly improve accuracy. Based on these findings, the 2 cm grid size was selected for the numerical model to analyze the pile scour process under the combined influence of waves and currents. Based on these findings, the 2 cm grid size was selected for the numerical model to analyze the pile scour process under the combined influence of waves and currents.

The developed numerical model is highly effective in predicting the temporal development of scour around circular piles in combined wave-current flows. The numerical model provides R^2 value of 0.991 and an index of agreement of 0.995, which shows an excellent fit to experimental data of Lyu et al. (2021). The *RMSE* value of 0.014 means that the average prediction error is very small, and the *NSE* of 0.981 suggests that the model's predictions are very close to the observed scour depths. These metrics suggest that the developed CFD model is a reliable tool for predicting scour development, making it useful for both research and practical applications in coastal and marine engineering.

3. Results and discussion

The validated CFD model is utilized to analyze the submerged pile scour with varying submergence ratios (h_c/D), where h_c is the height of the square pile above the bed. The consideration of submergence ratios (h_c/D) is primarily motivated by the findings of Zhao et al. (2010), in which no scour was observed for $h_c/D \leq 0.5$, attributed to the lack of vortex shedding, and the scour depth becomes independent of h_c for $h_c/D > 2$ in a steady flow. The absolute pile height (h_c) significantly affects the scour depth formation around the pile in wave-current flow. However, the normalization of pile height to the diameter facilitates the understanding of hydrodynamic similarity and scaling effects. This method provides a generalizable and robust framework for analyzing scour around submerged piles. Therefore, the present numerical study is performed for four h_c/D values of 0.5, 1, 1.5, and 2 and three different KC numbers of 5, 12, and 18. In this context, $KC = 5$ indicates the flow regime where no vortex shedding was observed. At the same time, $KC = 12$ and 18 represent the flow regimes where vortex shedding governs the scour phenomena for an unsubmerged square pile, as Sumer et al. (1993) suggested.

Throughout all the numerical tests, the water depth was maintained at 0.3 m. All the numerical simulations are performed using the wavelength (L) = 8.78 m. The wave parameters such as wave height (H), wave period (T), and wavelength are kept constant for each KC number, and the current velocity (U_c) is varied to obtain different U_{cw} values. In the present study, the U_{cw} parameters were systematically varied to maintain a fixed KC number. The variations included (a) $U_{cw} = 0$, representing waves alone; (b) $U_{cw} = 0.2$, indicating waves combined with weak currents; (c) $U_{cw} = 0.4$, indicating waves combined with mild currents; and (d) $U_{cw} = 0.6$, indicating waves combined with strong currents. The uniform median sediment grain size (d_{50}) of 0.18 mm was used for all the numerical tests. The critical Shields parameter (θ_{cr}) was kept constant at 0.047 in all the numerical simulations. In combined wave-current flow, the Ursell number plays a significant role in determining the appropriate wave theory. The Ursell number (U_r) is a dimensionless parameter used to identify the most applicable wave theory based on the wave characteristics. The Ursell number is defined as given in Eq. (14).

$$U_r = \frac{HL^2}{h^3} \tag{14}$$

where H represents the wave height, L is the wavelength, and h denotes the water depth.

According to Hedges (1995), fifth-order Stokes theory is applicable for $U_r < 40$, while fifth-order Cnoidal wave theory is preferable for higher values of the Ursell number (U_r). In the present study, the Ursell number varies between 78 and 133. Therefore, Cnoidal wave theory is applicable for all the numerical simulations. To simulate scour mechanism around the submerged square pile, an NWT of dimensions 5 m length, 1 m width, and 0.8 m depth is utilized. Using the relaxation approach at the inlet of NWT, waves can be generated within the NWTs (Jacobsen et al., 2011). Additionally, the Active Wave Absorption (AWA) technique is adopted at the NWT outlet to prevent wave reflection (Dutta et al., 2023). To simulate combined wave-current condition in NWT, Dirichlet boundary condition is applied at the inlet. The top surface of the NWT is considered as free surface and the no slip condition is applied at the sediment bed. The three dimensional computational domain of the NWT is shown in Fig. 8.

A total of 48 numerical simulations were performed to examine the submerged pile scour in wave-current flows. All the simulations achieve the equilibrium scour depth within 3600 s, denoted as T_e. A summary of the hydraulic and wave parameters employed in the numerical simulations is presented in (Table 2a, 2b, 2c, 2d).

3.1. Bed topography contours

Bed topography contours, serving as visual representations of changes in the bed elevation, are instrumental in unraveling the intricacies of scour phenomena. The study discusses the scour pattern around the submerged square pile for various h_c/D and U_{cw} parameters for a fixed $KC = 5$, 12, and 20.

Fig. 9 shows the bed topography contours around the submerged square pile for various h_c/D and U_{cw} parameters for a fixed $KC = 5$. In Fig. 9, the variation of h_c/D is shown from top to bottom (column-wise), indicating the value between 0.5 and 2, and the variation of Ucw is shown from left to right (row-wise), indicating the value between 0 and 0.6. The blue regions have negative values, denoting scour, while the red area indicates positive values, signifying sediment deposition around the submerged square pile. A symmetric scour at the upstream and deposition pattern at the downstream edges of the submerged square pile are observed, respectively. In wave-only conditions ($U_{cw} = 0$), when h_c/D is equal to 0.5 (Fig. 9(a)), the minimum scour depth is observed at the upstream edges, and deposition begins just after the scour hole, extending to the downstream edges of the submerged square pile. The more significant scour depth formation was observed around the upstream corners of the submerged square pile compared to the upstream center (stagnation point). This implies that flow accelerations at the upstream corners had a more significant impact on local scour than the HSV in front of the pile, as indicated by Zhao et al. (2012).

Further, the increase in h_c/D value increases the scour hole in all the

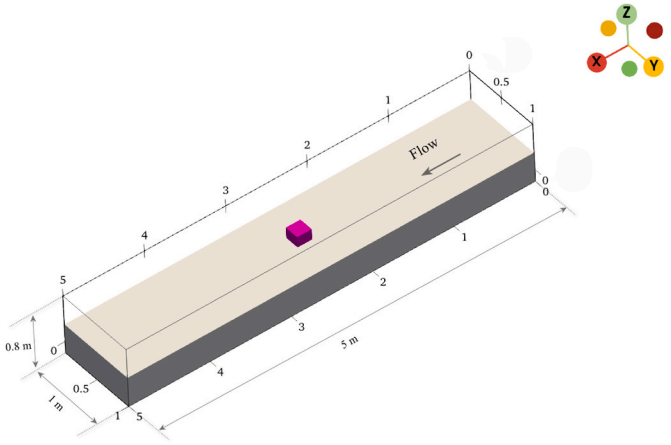

Fig. 8. The three-dimensional computational domain of NWT.

Table 2a
Numerical simulation results for submerged square pile ($h_c/D = 2$).

Sl. no.	D (m)	hc/D	H (m)	T (s)	U_w (m/s)	U_c (m/s)	U_{cw}	Fr_a	KC	U_r	S/D
1	0.14	2	0.065	4.5	0.156	0	0.0	0.085	5	78.29	0.0113
2	0.14	2	0.065	4.5	0.156	0.039	0.2	0.118	5	78.29	0.0168
3	0.14	2	0.065	4.5	0.156	0.104	0.4	0.173	5	78.29	0.0760
4	0.14	2	0.065	4.5	0.156	0.234	0.6	0.284	5	78.29	0.1776
5	0.10	2	0.111	4.5	0.267	0	0.0	0.172	12	133.70	0.1323
6	0.10	2	0.111	4.5	0.267	0.067	0.2	0.239	12	133.70	0.1748
7	0.10	2	0.111	4.5	0.267	0.178	0.4	0.351	12	133.70	0.1860
8	0.10	2	0.111	4.5	0.267	0.400	0.6	0.575	12	133.70	0.2695
9	0.06	2	0.1	4.5	0.240	0	0.0	0.199	18	120.45	0.2015
10	0.06	2	0.1	4.5	0.240	0.060	0.2	0.277	18	120.45	0.2249
11	0.06	2	0.1	4.5	0.240	0.160	0.4	0.408	18	120.45	0.2324
12	0.06	2	0.1	4.5	0.240	0.360	0.6	0.668	18	120.45	0.2852

Table 2b
Numerical simulation results for submerged square pile scour ($h_c/D = 1.5$).

Sl. no.	D (m)	hc/D	H (m)	T (s)	U_w (m/s)	U_c (m/s)	U_{cw}	Fr_a	KC	U_r	S/D
1	0.14	1.5	0.065	4.5	0.156	0	0.0	0.085	5	78.29	0.0094
2	0.14	1.5	0.065	4.5	0.156	0.039	0.2	0.118	5	78.29	0.0126
3	0.14	1.5	0.065	4.5	0.156	0.104	0.4	0.173	5	78.29	0.0665
4	0.14	1.5	0.065	4.5	0.156	0.234	0.6	0.284	5	78.29	0.1515
5	0.10	1.5	0.111	4.5	0.267	0	0.0	0.172	12	133.70	0.1316
6	0.10	1.5	0.111	4.5	0.267	0.067	0.2	0.239	12	133.70	0.1595
7	0.10	1.5	0.111	4.5	0.267	0.178	0.4	0.351	12	133.70	0.1773
8	0.10	1.5	0.111	4.5	0.267	0.400	0.6	0.575	12	133.70	0.2191
9	0.06	1.5	0.1	4.5	0.240	0	0.0	0.199	18	120.45	0.1789
10	0.06	1.5	0.1	4.5	0.240	0.060	0.2	0.277	18	120.45	0.2114
11	0.06	1.5	0.1	4.5	0.240	0.160	0.4	0.408	18	120.45	0.2262
12	0.06	1.5	0.1	4.5	0.240	0.360	0.6	0.668	18	120.45	0.2415

Table 2c
Numerical simulation results for submerged square pile scour ($h_c/D = 1$).

Sl. no.	D (m)	hc/D	H (m)	T (s)	U_w (m/s)	U_c (m/s)	U_{cw}	Fr_a	KC	U_r	S/D
1	0.14	1	0.065	4.5	0.156	0	0.0	0.085	5	78.29	0.0047
2	0.14	1	0.065	4.5	0.156	0.039	0.2	0.118	5	78.29	0.0070
3	0.14	1	0.065	4.5	0.156	0.104	0.4	0.173	5	78.29	0.0484
4	0.14	1	0.065	4.5	0.156	0.234	0.6	0.284	5	78.29	0.1188
5	0.10	1	0.111	4.5	0.267	0	0.0	0.172	12	133.70	0.1091
6	0.10	1	0.111	4.5	0.267	0.067	0.2	0.239	12	133.70	0.1291
7	0.10	1	0.111	4.5	0.267	0.178	0.4	0.351	12	133.70	0.1584
8	0.10	1	0.111	4.5	0.267	0.400	0.6	0.575	12	133.70	0.1730
9	0.06	1	0.1	4.5	0.240	0	0.0	0.199	18	120.45	0.1183
10	0.06	1	0.1	4.5	0.240	0.060	0.2	0.277	18	120.45	0.1332
11	0.06	1	0.1	4.5	0.240	0.160	0.4	0.408	18	120.45	0.1596
12	0.06	1	0.1	4.5	0.240	0.360	0.6	0.668	18	120.45	0.1991

Table 2d
Numerical simulation results for submerged square pile scour ($h_c/D = 0.5$).

Sl. no.	D (m)	hc/D	H (m)	T (s)	U_w (m/s)	U_c (m/s)	U_{cw}	Fr_a	KC	U_r	S/D
1	0.14	0.5	0.065	4.5	0.156	0	0.0	0.085	5	78.29	0.0013
2	0.14	0.5	0.065	4.5	0.156	0.039	0.2	0.118	5	78.29	0.0043
3	0.14	0.5	0.065	4.5	0.156	0.104	0.4	0.173	5	78.29	0.0320
4	0.14	0.5	0.065	4.5	0.156	0.234	0.6	0.284	5	78.29	0.0810
5	0.10	0.5	0.111	4.5	0.267	0	0.0	0.172	12	133.70	0.0204
6	0.10	0.5	0.111	4.5	0.267	0.067	0.2	0.239	12	133.70	0.0237
7	0.10	0.5	0.111	4.5	0.267	0.178	0.4	0.351	12	133.70	0.0933
8	0.10	0.5	0.111	4.5	0.267	0.400	0.6	0.575	12	133.70	0.1026
9	0.06	0.5	0.1	4.5	0.240	0	0.0	0.199	18	120.45	0.0580
10	0.06	0.5	0.1	4.5	0.240	0.060	0.2	0.277	18	120.45	0.1451
11	0.06	0.5	0.1	4.5	0.240	0.160	0.4	0.408	18	120.45	0.2135
12	0.06	0.5	0.1	4.5	0.240	0.360	0.6	0.668	18	120.45	0.2386

directions at the upstream edges of the submerged square pile in wave-only conditions (Fig. 9(e), (i), and (m)) and hence maximum scour depth is observed for $h_c/D = 2$ (Fig. 9(m)). This increase in scour depth around the submerged square pile with an increase in h_c/D value is mainly attributed to the development of a larger and stronger HSV, as Dey et al. (2008) reported. While investigating the influence of the submerged square pile, it is noteworthy that the pattern of scour and deposition remains almost similar for all h_c/D values in wave-only conditions at *KC*

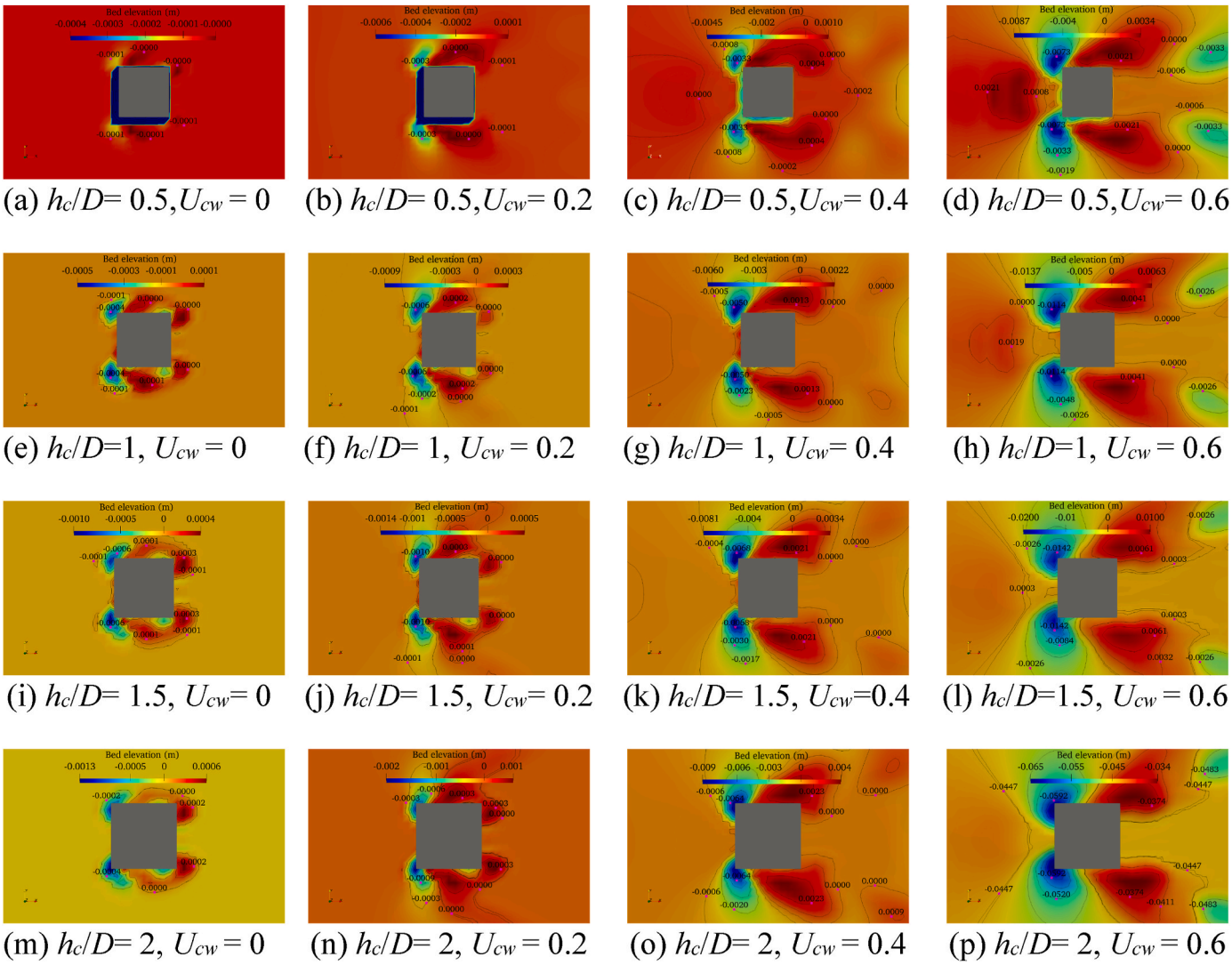

Fig. 9. Bed topography contours around the submerged square pile for various h_c/D and U_{cw} parameters for a fixed KC = 5.

= 5. When the waves are combined with weak currents (U_{cw} = 0.2), a larger and wider scour depth formation is observed around the submerged square pile (Fig. 9(b)) compared to wave-only conditions for h_c/D. = 0.5. The increased scour depth around a submerged square pile is primarily attributed to the introduction of an extra dynamic current component. This additional current significantly influences sediment transport and scour processes, enhancing flow pattern complexity and resulting in a more extensive scour around the pile due to the interaction between waves and currents. Further, an increase in the h_c/D value (Fig. 9(f), (j), and (n)) leads to the development of larger and wider scour hole formations at the upstream edges of the submerged square pile, similar to U_{cw} = 0. The superimposition of waves over mild current (U_{cw} = 0.4) increases the maximum scour depth and extends the scour hole reach around the submerged square pile (Fig. 9(c), (g), (k) and (o)) compared to U_{cw} = 0 and 0.2 conditions. It can also be observed that sand deposition extends its reach downstream of the submerged square pile. Further, superimposition of waves over strong current (U_{cw} = 0.6) results in the formation of larger and wider scour depths upstream of the submerged pile, accompanied by a lengthy, elongated deposition of sand in flow direction followed by the formation of wing scour hole downstream of the submerged pile (Fig. 9(d), (h), (l) and (p)). Similar to wave-alone conditions, the pattern of scour and deposition around the submerged square pile remains nearly identical for all h_c/D values at KC = 5 for a particular U_{cw} value in combined wave-current flows. Notably, the maximum scour depth is observed for h_c/D = 2 across all U_{cw} parameters (Fig. 9(m), (n), (o), and (p)), for a fixed KC = 5, primarily due to the formation of more pronounced downflow and strong HSV.

Fig. 10 represents the bed topography contours around the submerged square pile for various h_c/D and U_{cw} parameters for a fixed KC = 12. A symmetric scour at the upstream and deposition pattern at the downstream edges of the submerged square pile are observed at KC = 12. In the wave-only conditions (U_{cw} = 0), when h_c/D is equal to 0.5 (Fig. 10(a)), the minimum scour depth is observed at the upstream edges, and no deposition of sand is observed around the submerged square pile. With the increase in the U_{cw} parameter, a gentle increase in the scour hole at the upstream edges can be observed (Fig. 10(b–d)). In the presence of waves combined with a strong current (U_{cw} = 0.6) at h_c/D=0.5 (Fig. 10(d)), sand deposition occurs upstream of the pile, while the maximum scour hole is observed downstream of the pile. The deposition in front of the pile is attributed to reduced downflow and the development of a weak HSV, primarily resulting from the lower height of the cylinder. However, the occurrence of larger scour is primarily attributed to the influence of a robust trailing vortex, which mitigates the lateral wakes. According to Tafarojnoruz and Lauria (2020), these lateral wakes are suppressed by reducing the upward velocity component of the wake vortices created at the cylinder sidewalls in the top section of the pile wake. Further, the increase in h_c/D value increases the scour hole at the upstream edges of the submerged square pile in the

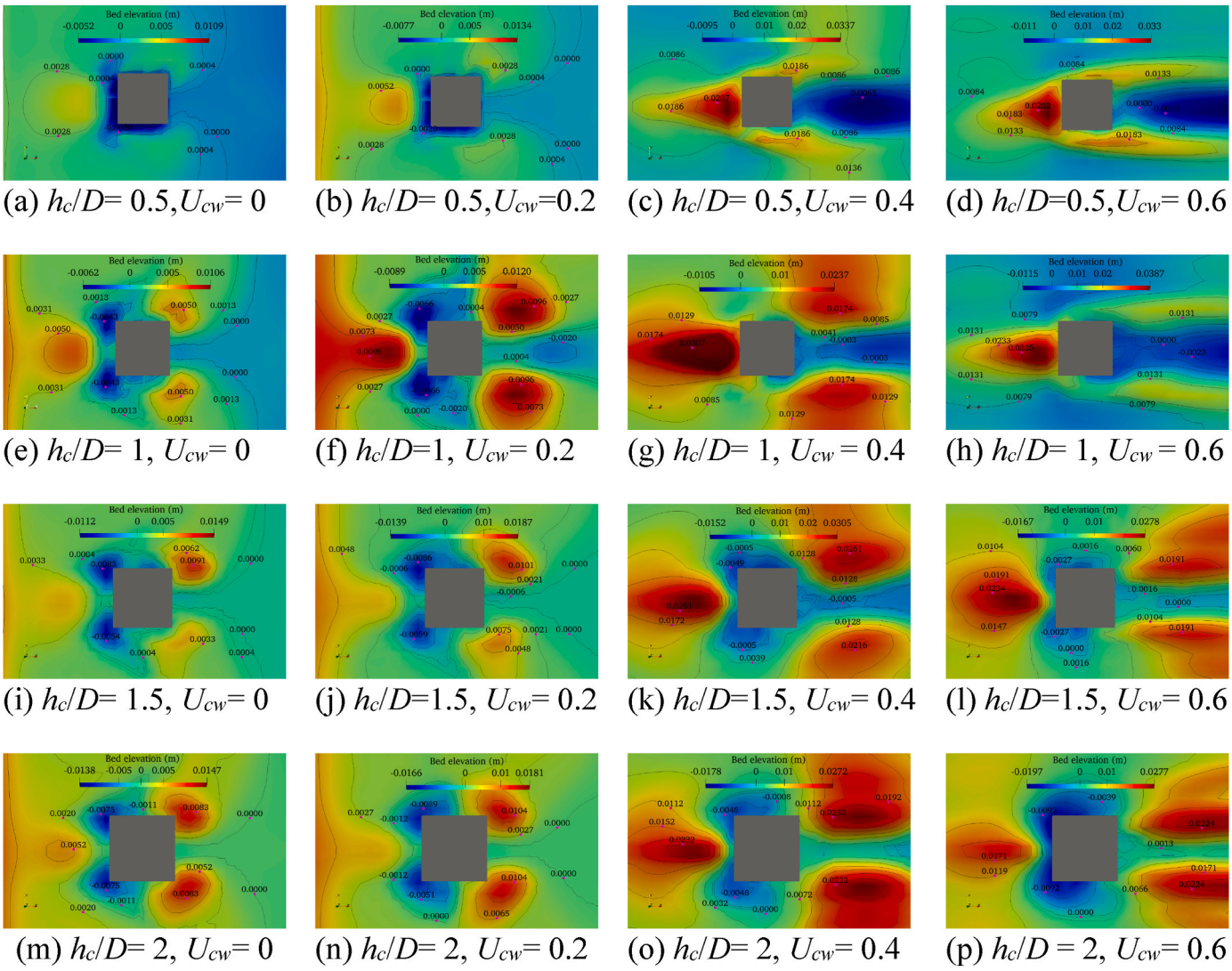

Fig. 10. Bed topography contours around the submerged square pile for various h_c/D and U_{cw} parameters for a fixed KC = 12.

wave-only conditions and combined wave-current flows (Fig. 10(e–p). This increase in scour depth around the submerged square pile with an increase in h_c/D value is mainly attributed to the development of a larger downflow and strong HSV, as Dey et al. (2008) reported.

Fig. 11 represents the bed topography contours around the submerged square pile for various h_c/D and U_{cw} parameters for a fixed KC = 18. Similar to KC = 5 and 12, a symmetric scour at upstream and deposition pattern at the downstream edges of the submerged square pile is observed at KC = 18. In wave-only conditions (U_{cw} = 0), when h_c/D is equal to 0.5 (Fig. 11(a)), the minimum scour depth is observed just behind the submerged square pile, and deposition of sand is observed upstream of the submerged square pile. With the increase in the U_{cw} parameter, a gentle rise in the scour hole at the downstream center can observed (Fig. 11(b–d)). In the presence of waves combined with a strong current (U_{cw} = 0.6) at h_c/D=0.5 (Fig. 11 (d)), significant sand deposition occurs upstream of the pile, while the maximum scour hole is observed downstream of the pile. The deposition in front of the pile in the case of a smaller height (h_c/D = 0.5) is attributed to the reduced downflow velocities and the development of a weak HSV. However, the occurrence of larger scour is attributed mainly to the influence of a robust trailing vortex, which mitigates the lateral wakes similar to KC = 12. In wave-only conditions, the oscillatory motion creates a stagnation zone in front of the pile, reducing flow velocity and leading to upstream sediment accumulation. Further, the vortex shedding and flow reversal enhance this deposition upstream of the submerged pile. In combined wave-current conditions, the dominant wave forces weaken the current's effect, causing similar sediment accumulation upstream. However, for larger U_{cw} values, the current parameter dominates the flow, leading to larger scour depth formation around the submerged pile. For the wave-only condition at h_c/D = 1 (Fig. 11 (e)), the deposition pattern in front of the pile is almost similar to the wave-only condition at h_c/D = 0.5. Further, the scour pattern is almost similar to h_c/D = 0.5 in combined wave-current conditions. At h_c/D = 1.5, initially, the upstream edge scour holes can be observed in wave-only conditions (Fig. 11 (i)). However, as the U_{cw} value increases, the deposition starts dominating at the upstream edges of the pile, and finally, the larger deposition can be observed at the upstream edges and scour in downstream of the pile in case of U_{cw} = 0.6 (Fig. 11 (l)). An almost similar pattern of scour and deposition can be observed in the case of h_c/D = 2.

The submergence ratio is an essential parameter that affects the bed profiles due to the development of trailing vortices. A higher submergence ratio, where the top surface of the pile is much closer to the water surface, results in more stable flow patterns around the pile and poses less impact on the bed surface. However, more complex flow patterns and stronger asymmetrical trailing vortices are developed for lower submergence ratios. These asymmetrical trailing vortices can affect the shear stress and turbulence patterns around the pile (McKenna Neuman et al., 2013). Therefore, these strong and asymmetric trailing vortices at

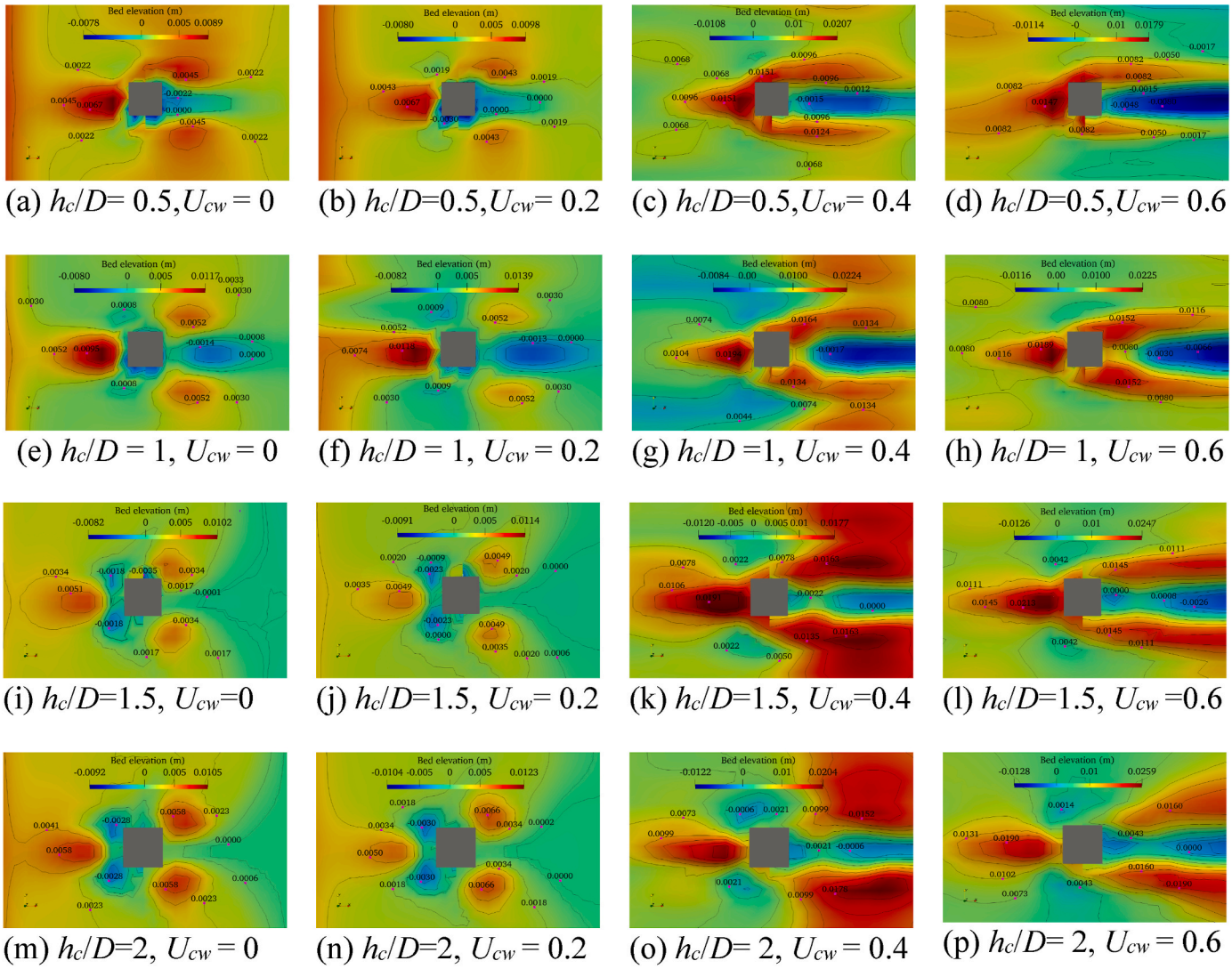

Fig. 11. The bed topography contours around the submerged square pile for various h_c/D and U_{cw} parameters for a fixed KC = 18.

lower submergence ratios lead to more pronounced and irregular scour patterns. Further, the flow regimes also affect the sediment transport in wave-only conditions. According to Sumer and Fredsøe (2002), different flow regimes can be observed around the pile based on the *KC* number. They reported that the symmetrical tail eddies are formed downstream of the pile for *KC* numbers between 2.8 and 4, whereas these eddies become asymmetrical for *KC* numbers between 4 and 6. For KC numbers between 6 and 17, vortex shedding occurs on only one side of the pile per half cycle of the wave. For KC numbers between 17 and 23, alternating vortex shedding patterns develop and spread to the rear side of the pile. In the present study, the bed topography was examined for three different *KC* numbers 5, 12, and 18. An asymmetrical scour and deposition patterns can be observed for $KC = 5$, which is mainly due to the flow regime causing asymmetrical eddies for *KC* number equal to 5. For $KC = 12$, one-sided vortex shedding further disrupts symmetry. For $KC = 18$, alternating vortex shedding contributes to the complex and asymmetrical patterns observed around the pile.

In both wave-only and combined wave-current conditions with higher Keulegan-Carpenter (*KC*) numbers, such as 12 and 18, a sediment deposition upstream of a submerged square pile can be observed. In wave-only conditions, the oscillatory motion creates a stagnation zone in front of the pile where the flow velocity is significantly reduced, limiting sediment transport and causing sand to settle upstream in the case of higher *KC* numbers such as 12 and 18. Further, vortex shedding and the flow reversal during the wave cycle further contribute to periodic deceleration, enhancing deposition. Similarly, in combined wave-current conditions, the interaction between the waves and the steady current weakens the current's influence, with wave forces becoming dominant, leading to similar upstream sediment accumulation. Additionally, cyclic pressure gradients induced by waves push sediment toward the upstream face of the pile, and the suppression of current-induced scour in high *KC* regimes allows for greater deposition in the upstream region. These combined effects are responsible for the observed sediment deposition in upstream of submerged square pile in wave-only and combined wave-current conditions.

3.2. Temporal variation of scour

The progression of maximum equilibrium scour depth around a pile involves distinct stages, as Hong et al. (2012) described: initial scouring, developing scouring, and equilibrium scouring. In the initial scouring phase, scour depth is rapidly developed. Subsequently, the developing scouring stage is characterized by a more prolonged duration, contingent upon the prevailing clear-water or live-bed scour regimes. Finally, in the equilibrium scouring stage, the scour depth either remains constant in clear-water scour conditions or exhibits a moderate fluctuation in live-bed scour conditions, as detailed by Melville and Chiew (1999).

Fig. 12 depicts the temporal variation of *S/D* at submerged square

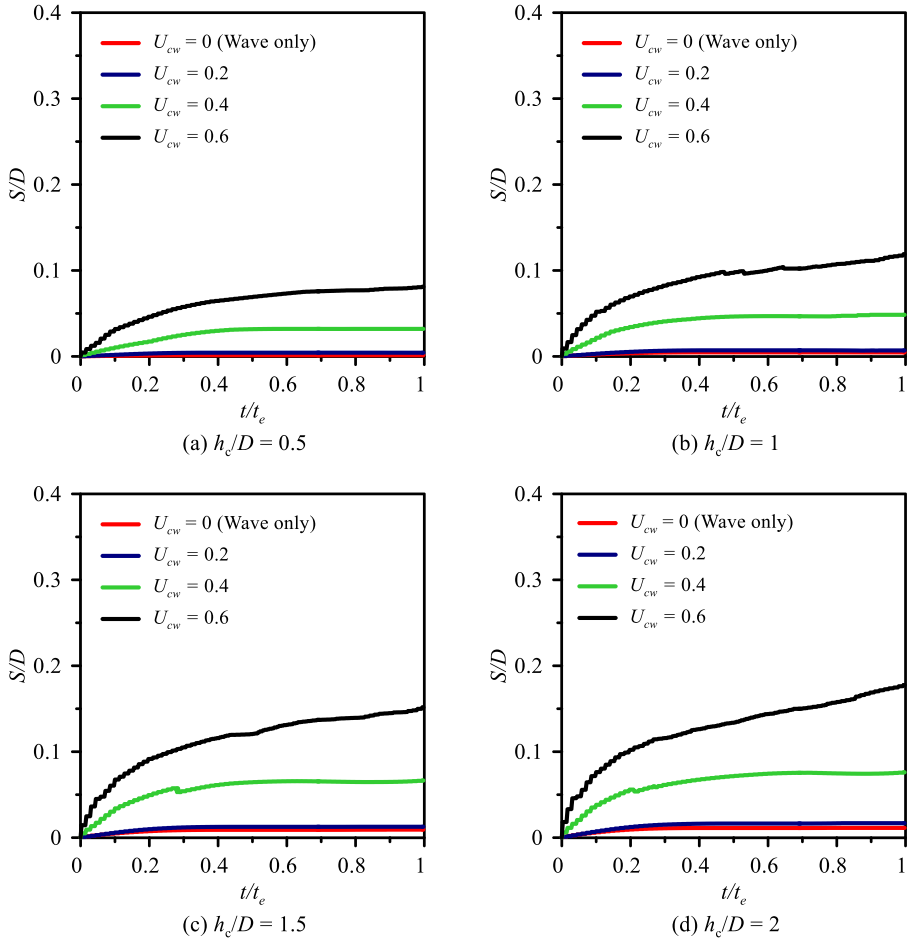

Fig. 12. Temporal variation of normalized scour depth (S/D) at different h_c/D for a fixed $KC = 5$.

piles under different U_{cw} and h_c/D parameters for $KC = 5$. At fixed h_c/D=0.5 (Fig. 12(a)), the minimum and maximum values of S/D were observed at $U_{cw} = 0$ and $U_{cw} = 0.6$, respectively. In wave-only conditions ($U_{cw} = 0$), the occurrence of minimum scour hole is mainly attributed to the generation of smaller HSV around the submerged pile, as Gautam et al. (2021) suggested. Further, the increase in the U_{cw} parameter increases the scour depth around the submerged pile. This is mainly due to the introduction of the dynamic current component in the combined wave-current flow. This additional current significantly influences the development of HSV, and thus, an increase in scour depth can be observed in combined wave-current flows. Therefore, the maximum scour depth can be observed for $U_{cw} = 0.6$ at $h_c/D = 0.5$. Further, the temporal evolution of submerged pile scour was observed at $h_c/D = 1$ (Fig. 12(b)), $h_c/D = 1.5$ (Fig. 12(c)) and $h_c/D = 2$ (Fig. 12(d)), while maintaining a constant value of $KC = 5$. With the increase in h_c/D, the rise in S/D value can be observed in Fig. 12. This increase in scour depth around the submerged square pile with an increase in h_c/D value, is mainly attributed to the development of a larger and stronger HSV, as reported by Dey et al. (2008).

Fig. 13 depicts the temporal variation of S/D at submerged square piles under different U_{cw} and h_c/D parameters for $KC = 12$. Similar to $KC = 5$, at fixed h_c/D=0.5 (Fig. 13(a)), the minimum and maximum values of S/D were observed at $U_{cw} = 0$ and $U_{cw} = 0.6$, respectively. It can be observed that the increase in the U_{cw} parameter increases the S/D values for a fixed value of h_c/D, which is mainly due to stronger HSV and lee-wake vortex. The vortex shedding regulates the scour phenomena when $KC > 11$ in unsubmerged square piles. However, in a submerged square pile, the downstream vortex shedding is entirely suppressed by the developed trailing vortex. Further, the temporal evolution of submerged pile scour was observed at $h_c/D = 1$ (Fig. 13(b)), $h_c/D = 1.5$ (Fig. 13(c)) and $h_c/D = 2$ (Fig. 13(d)), while maintaining a constant value of $KC = 12$. It can be observed that with an increase in h_c/D, the scour depth also increases for fixed U_{cw} parameters, which is mainly due to the development of larger downflow, HSV, and wake vortices, as suggested by Dey et al. (2008). Additionally, it becomes apparent that an increase in the KC number leads to higher scour depths across various h_c/D parameters.

Fig. 14 depicts the temporal variation of S/D at submerged square piles under different U_{cw} and h_c/D parameters for $KC = 18$. Similar to $KC = 5$ and 12, at fixed h_c/D=0.5 (Fig. 14(a)), the minimum and maximum values of S/D were observed at $U_{cw} = 0$ and $U_{cw} = 0.6$, respectively. Similar patterns of scour development are observed for different h_c/D values, as shown in Fig. 14(b–d). Similar to $KC = 5$ and 12, the increase in scour depth can be observed with an increase in the U_{cw} parameter for a fixed value of h_c/D. However, for the h_c/D value from 1 to 2, a mild increase in scour depth can be observed, along with an increase in the U_{cw} parameter at $KC = 18$. For a given U_{cw} value, it can be observed that the S/D value increases as the h_c/D value increases. This is mostly due to the generation of strong HSV and downflow, as suggested by Dey et al. (2008).

3.3. Effect of KC number and U_{cw} on scour depth

In the context of pile scour under combined wave-current flows, KC number and U_{cw} parameters are the most essential parameters, as reported by Sumer and Fredsøe (2001). The findings of Sumer and Fredsøe (2001) analysis are also supported by Qi and Gao (2014a) experimental investigation. Therefore, the effect of KC numbers (5, 12, and 18) and

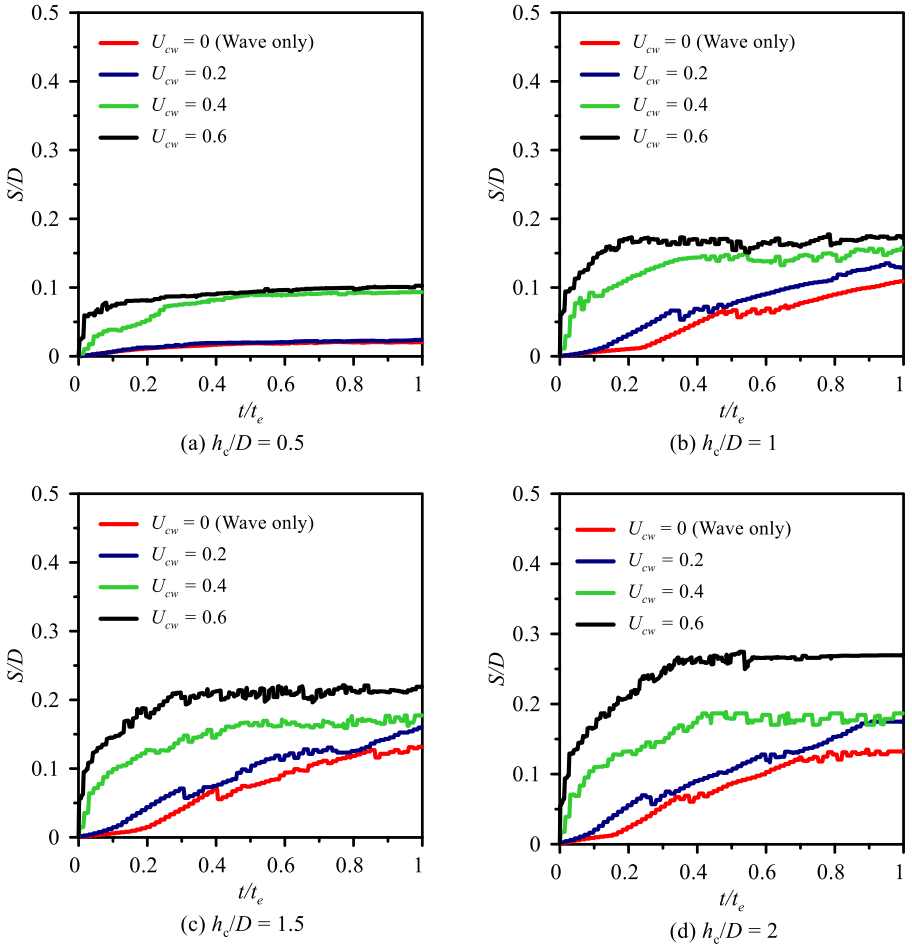

Fig. 13. Temporal variation of normalized scour depth (S/D) at different h_c/D for a fixed KC = 12.

U_{cw} parameters (0, 0.2, 0.4, and 0.6) on S/D values of submerged square piles are shown in Fig. 15.

Fig. 15(a) shows the variation of S/D with different U_{cw} parameters for a submerged square pile ($h_c/D = 0.5$) at different KC values. It can be observed that the U_{cw} significantly affects the S/D values for low KC values, particularly at $KC = 5$. The low KC regime shows a substantial rise in S/D values as U_{cw} increases from 0 to 0.4. Additionally, an increase in U_{cw} values from 0.4 to 0.6 results in a moderate S/D increment for low KC numbers. This occurs because a stronger HSV consistently develops in front of the pile, even when the current is relatively weak. Further, at $KC = 12$, a mild increase in the S/D value can be observed with an increase in the U_{cw} parameter for $h_c/D = 0.5$. However, in a higher KC regime (e.g., $KC = 18$), the influence of U_{cw} on scour depth becomes less significant. For instance, an increase in U_{cw} from 0 to 0.2 shows a gradual rise in S/D values for a higher KC regime at $h_c/D = 0.5$. Nevertheless, the normalized scour depth remains relatively constant as U_{cw} values increase from 0.2 to 0.6. For a given U_{cw}, it can be seen that an increase in the KC number increases the S/D values at the submerged square pile. The present study findings are consistent with previous research conducted by Sumer and Fredsøe (2001), validating the influence of U_{cw} and KC numbers on S/D.

Sumer and Fredsøe (2002) discussed different flow regimes around the pile based on the KC number in wave-only conditions. They reported that the symmetrical tail eddies are formed downstream of the pile for KC numbers between 2.8 and 4, whereas these eddies become asymmetrical for KC numbers between 4 and 6. For KC numbers between 6 and 17, vortex shedding occurs only on one side of the pile per half cycle of the wave, and for KC numbers between 17 and 23, vortex shedding alternates sides, spreading to the rear of the pile.

In wave-only conditions, the KC number significantly impacts scour depth around a submerged square pile. At lower KC value, a smaller horseshoe vortex exists and does not have much effect on the scouring process (Sumer et al. 1997). However, as the KC value increases, the horseshoe vortex becomes more prominent and plays a significant role in the scouring process, eventually becoming the dominant factor when KC exceeds 100 (Sumer et al., 1992). For the situation of a lower KC value, the presence of the horseshoe vortex in both space and time is very limited (Sumer et al. 1997); therefore, its influence on the scour will not be significant. However, the rate of erosion is faster in these lower KC regimes compared to larger KC numbers, because the oscillatory flow effects are more pronounced and eddies become asymmetrical, leading to more dynamic sediment transport and erosion around the submerged pile. As the KC number increases to moderate levels (KC = 12), the wave-induced orbital velocities and associated kinetic energy rise, resulting in more significant sediment transport and a faster rate of scour development due to vortex shedding occurring only on one side of the pile per half cycle of the wave. In high KC regimes ($KC = 18$), while the wave forces are stronger and produce higher wave-induced orbital velocities leading to greater overall scour depth, the rate of erosion actually becomes lower. This is because the scour process approaches an equilibrium state more quickly due to the high energy input from the waves, stabilizing the sediment transport around the submerged pile.

Fig. 15(b) shows the variation of S/D with different U_{cw} parameters for submerged square piles ($h_c/D = 1$) at different KC values. Similar to the $h_c/D = 0.5$, a significant rise in the S/D values can be observed as the U_{cw} parameters vary from 0 to 0.4 for low KC numbers of 5. Further, an increase in U_{cw} values from 0.4 to 0.6 shows a moderate increase in S/D values at the low KC numbers of 5. Additionally, as the KC number

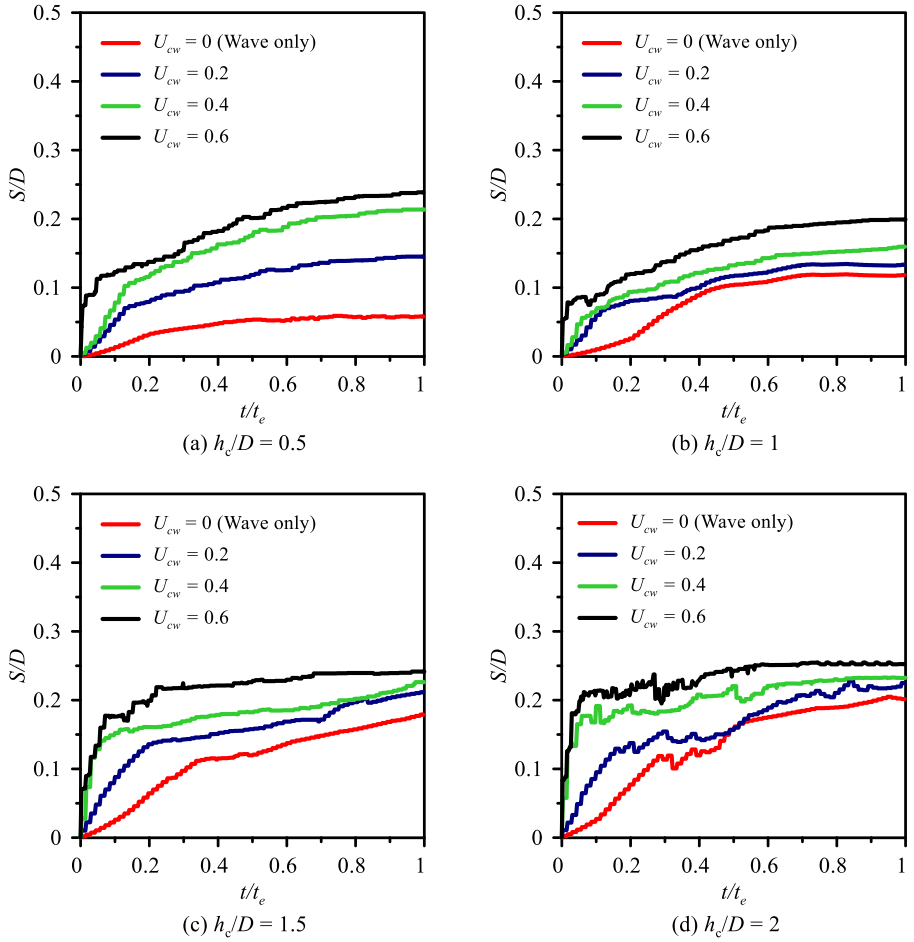

Fig. 14. Temporal variation of normalized scour depth (S/D) at different h_c/D for a fixed $KC = 18$.

increases to 12, a mild increase in the S/D value is observed. At this point, a gradual increase in the S/D value is observed with a corresponding rise in U_{cw} values. As the KC number increases to 18, no significant effect on the S/D values was observed compared to the $KC = 12$. A similar variation of S/D can be observed for h_c/D equal to 1.5 (Fig. 15 (c)) and 2 (Fig. 15(d)) at submerged square piles.

3.4. Influence of average-velocity-based Froude number (Fr_a)

The significance of the average-velocity-based Froude number (Fr_a) in establishing the equilibrium scour depth in wave-current flows was highlighted by Qi and Gao (2014b). The flow structures, such as HSV and wake vortices, are closely linked to the Fr_a, which is responsible for the scour development around a pile. The normalized scour depths around submerged square piles in wave-current flows, as a function of Fr_a for various h_c/D values, are shown in Fig. 16.

The analysis reveals a noticeable trend in the S/D value with respect to Fr_a. A rapid increase in the S/D value is observed for Fr_a values of 0–0.4. A further increase in Fr_a values from 0.4 to 1 results in an almost constant S/D value. Similarly, as the h_c/D parameter increases, the S/D value also increases for a constant Fr_a. However, h_c/D values of 1.5 and 2 show almost similar variations of S/D values. Qi and Gao (2014b) also observed a similar pattern of S/D around a square pile under combined wave-current flows. Moreover, when examining the specific case of h_c/D equal to 2, a higher S/D value is evident, as depicted by the corresponding fitting curve. Conversely, the minimum S/D value is observed for h_c/D equal to 0.5, as illustrated by its fitting curve.

4. Conclusions

Submerged square piles are the most common coastal structures that are built to support oil and gas rigs, and offshore platforms. The submerged piles are mainly designed to withstand the hydrodynamic forces induced by combined wave-current flows. The interaction of combined wave-current flows with the submerged pile can cause scour development around the pile, which can ultimately lead to structural failure. Therefore, the present study utilizes a three-dimensional numerical model to examine the scour phenomenon around the submerged square pile. Based on the analysis of the numerical results obtained in the present study, the following conclusions have been drawn.

- The increase in the pile height-to-width ratio (h_c/D) from 0.5 to 2 leads to an increase in the normalized equilibrium scour depth (S/D) from 0.0013 to 0.0113 under wave-only ($U_{cw} = 0$) conditions for a fixed $KC = 5$. Similar trend is also observed for U_{cw} values of 0.2, 0.4, and 0.6 at the $KC = 5$. This increase in scour depth is attributed to the larger downflow velocities around the pile as h_c/D increases, which enhance sediment transport and result in greater scour around the pile.
- The increase in the KC number from 5 to 18 leads to an increase in S/D from 0.0013 to 0.0580 under wave-only ($U_{cw} = 0$) conditions for a fixed $h_c/D = 0.5$. A similar trend is also observed in combined wave-current flow conditions for U_{cw} values of 0.2, 0.4, and 0.6 at the same h_c/D. This increase in scour depth is mainly due to the formation of stronger horseshoe vortices, which become the dominant factor in the scour process at higher KC values.

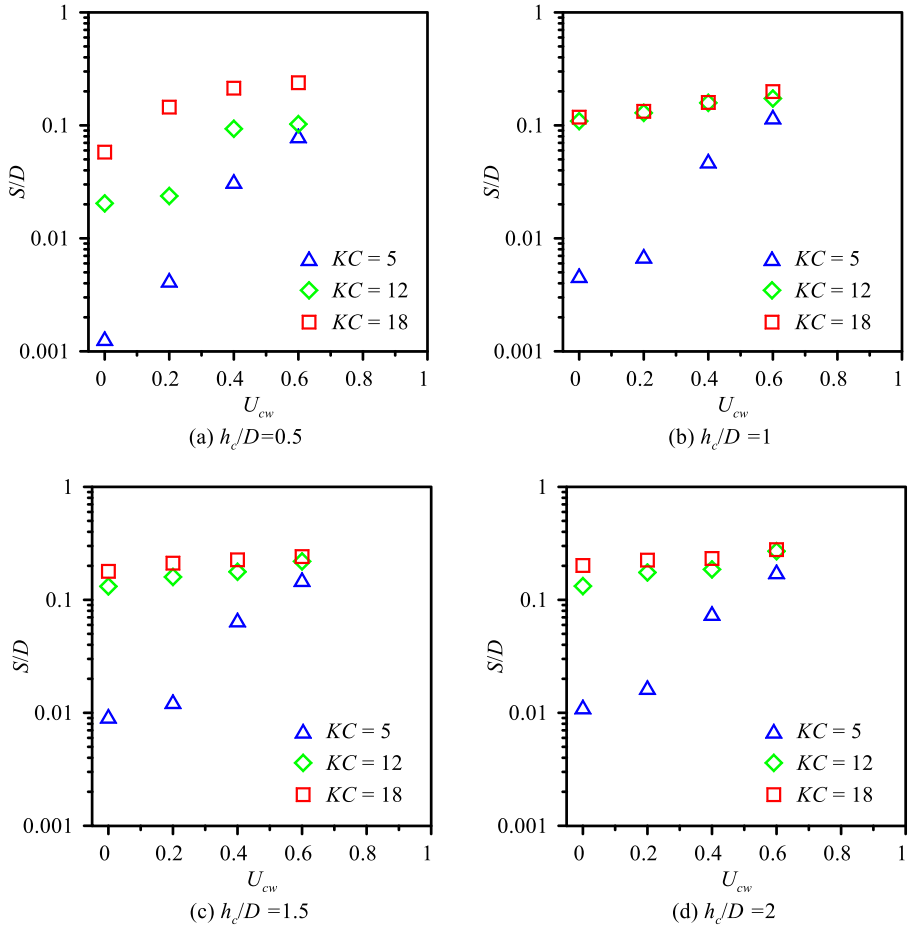

Fig. 15. Normalized scour depth (S/D) vs. (a) the wave-current parameters (U_{cw}) for square pile in different KC regimes for various h_c/D.

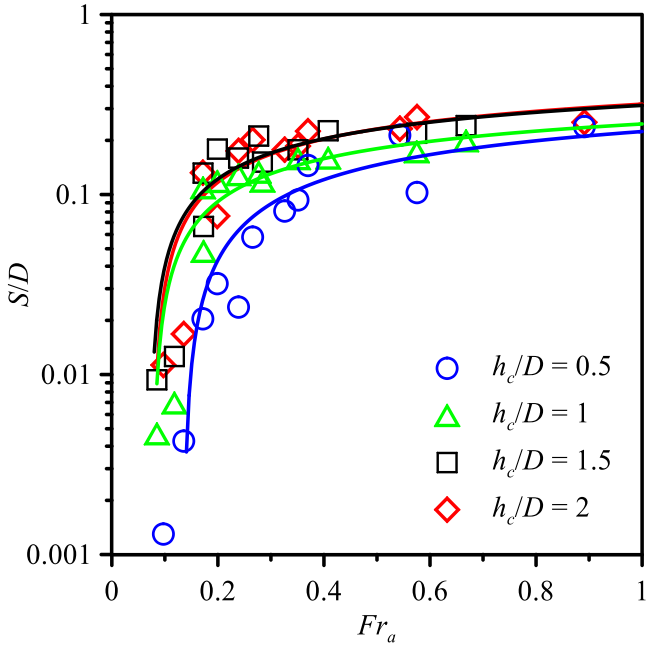

Fig. 16. Normalized scour depth (S/D) vs. the average-velocity-based pile Froude number (F_{ra}) for submerged square pile under combined wave-current flow.

- When waves are combined with weak or mild currents ($U_{cw} < 0.4$), a gentle increase of approximately 15–20% in the normalized equilibrium scour depth (S/D) is observed compared to wave-only conditions around the submerged square pile for low KC number ($KC = 5$). However, when waves are combined with strong currents ($U_{cw} = 0.6$), a more significant increase of up to 50% in the S/D values is observed compared to wave-only condition ($KC = 5$). This significant increase in scour depth for $U_{cw} = 0.6$ is predominantly due to the dominance of current forces over wave forces, which enhance turbulence and sediment mobilization around the pile.
- The effect of U_{cw} becomes negligible in higher KC regimes ($KC \geq 12$) compared to the low KC regime ($KC = 5$). This is because in higher KC regimes, wave forces dominate the scour process over the current forces. For larger KC values of 12 and 18, the U_{cw} parameters have less effect on scour depth. This is attributed to the suppression of lee-wake vortices by the development of trailing vortices.

CRediT authorship contribution statement

Lalit Kumar: Writing – original draft, Visualization, Validation, Software, Methodology, Investigation, Formal analysis, Data curation, Conceptualization. **Mohammad Saud Afzal:** Writing – review & editing, Writing – original draft, Validation, Supervision, Resources, Project administration, Methodology, Investigation, Funding acquisition, Formal analysis, Conceptualization. **Said Alhaddad:** Writing – review & editing, Supervision, Conceptualization.

Declaration of competing interest

The authors declare that they have no known competing financial interests or personal relationships that could have appeared to influence the work reported in this paper.

Acknowledgments

The present research is funded by the project "Computational Fluid Dynamics Modeling of Hydrodynamics and Scour around Coastal Structures", supported by the Science and Engineering Research Board (SERB), a division of the Department of Science and Technology in India. The research received funding under the grant number CRG/2022/002353. Additionally, the investigation benefited from the Super-computing facility at IIT Kharagpur.

References

Alhaddad, S., de Wit, L., Labeur, R.J., Uijttewaal, W., 2020. Modeling of breaching-generated turbidity currents using large eddy simulation. J. Mar. Sci. Eng. 8, 728.
Alhaddad, S., Keetels, G., Mastbergen, D., van Rhee, C., Lee, C.H., Puig Montellà, E., Chauchat, J., 2024. Subaqueous dilative slope failure (breaching): current understanding and future prospects. Adv. Water Resour. 188.
Alhaddad, S., Weij, D., van Rhee, C., Keetels, G., 2023. Stabilizing and destabilizing breaching flow slides. J. Mar. Sci. Eng. 11.
Bordbar, A., Sharifi, S., Hemida, H., 2021. Investigation of the flow behaviour and local scour around single square-shaped cylinders at different positions in live-bed. Ocean Eng. 238, 109772.
Burkow, M., Griebel, M., 2016. A full three dimensional numerical simulation of the sediment transport and the scouring at a rectangular obstacle. Comput. Fluid 125, 1–10.
Chen, B., Li, S., 2018. Experimental Study of Local Scour around a vertical cylinder under wave-only and combined wave-current conditions in a large-scale flume. J. Hydraul. Eng. 144, 4018058.
Chorin, A.J., 1968. Numerical solution of the Navier-Stokes equation. Math. Comput. 22, 745–762.
Dey, S., 2014. Fluvial Hydrodynamics. Springer.
Dey, S., 2003. Threshold of sediment motion on combined transverse and longitudinal sloping beds. J. Hydraul. Res. 41, 405–415.
Dey, S., Raikar, R.V., Roy, A., 2008. Scour at submerged cylindrical obstacles under steady flow. J. Hydraul. Eng. 134, 105–109.
Du, S., Wang, Z., Wang, R., Liang, B., Pan, X., 2022a. Effects of flow intensity on local scour around a submerged square pile in a steady current. Phys. Fluids 34.
Du, S., Wu, G., Zhu, D.Z., Wang, R., Lu, Y., Liang, B., 2022b. Experimental study of local scour around submerged square piles in combined waves and current. Ocean Eng. 266, 113176.
Durbin, P.A., 2009. Limiters and wall treatments in applied turbulence modeling. Fluid Dynam. Res. 41, 1–18.
Dutta, D., Afzal, M.S., Alhaddad, S., 2023. 3D CFD Study of Scour in Combined Wave–Current Flows Around Rectangular Piles with Varying Aspect Ratios. Water 15.
Eadie IV, R.W., Herbich, J.B., 1987. Scour about a single, cylindrical pile due to combined random waves and a current. In: Coastal Engineering 1986, pp. 1858–1870.
Engelund, F., Fredsoe, J., 1976. A sediment transport model for straight alluvial channels. Hydrol. Res. 7, 293–306.
Jacobsen, N.G., Fuhrman, D.R., Fredsøe, J., 2011. A wave generation toolbox for the open-source CFD library: OpenFOAM. Int. J. Numer. Methods Fluid.
Jiang, G.S., Shu, C.W., 1996. Efficient implementation of weighted ENO schemes. J. Comput. Phys. 126, 202–228.
Khosronejad, A., Arabi, M.G., Angelidis, D., Bagherizadeh, E., Flora, K., Farhadzadeh, A., 2020. A comparative study of rigid-lid and level-set methods for LES of open-channel flows: morphodynamics. Environ. Fluid Mech. 20, 145–164.
Khosronejad, A., Kang, S., Sotiropoulos, F., 2012. Experimental and computational investigation of local scour around bridge piers. Adv. Water Resour. 37, 73–85.
Kumar, L., Afzal, M.S., 2023. Experimental and numerical modelling of scour at vertical wall abutment under combined wave-current flow in low KC regime. Ocean Eng. 285, 115394.
Lancaster, O., Cossu, R., Wilson, M., Baldock, T.E., 2022. A 3D numerical and experimental parametric study of wave-induced scour around large bluff body structures. Ocean Eng. 266, 112766.
Lyu, X., Cheng, Y., Wang, W., An, H., Li, Y., 2021. Experimental study on local scour around submerged monopile under combined waves and current. Ocean Eng. 240, 109929.
McKenna Neuman, C., Sanderson, R.S., Sutton, S., 2013. Vortex shedding and morphodynamic response of bed surfaces containing non-erodible roughness elements. Geomorphology 198, 45–56.
Melville, B.W., Chiew, Y.-M., 1999. Time scale for local scour at bridge piers. J. Hydraul. Eng. 125, 59–65.
Mingham, C.G., Causon, D.M., 2000. Calculation of unsteady bore diffraction using a high resolution finite volume method. J. Hydraul. Res. 38, 49–56.
Naot, D., Rodi, W., 1982. Calculation of secondary currents in channel flow. J. Hydr. Div., ASCE 108, 948–968.
Osher, S., Sethian, J.A., 1988. Fronts propagating with curvature-dependent speed: algorithms based on Hamilton-Jacobi formulations. J. Comput. Phys. 79, 12–49.
Pedram, B., 2015. Effects of pile shape in improving the performance of monopiles embedded in onshore clays. Can. Geotech. J. 52, 1144–1158.
Qi, W.-G., Gao, F.-P., 2014a. Physical modeling of local scour development around a large-diameter monopile in combined waves and current. Coast. Eng. 83, 72–81.
Qi, W., Gao, F., 2014b. Equilibrium scour depth at offshore monopile foundation in combined waves and current. Sci. China Technol. Sci. 57, 1030–1039.
Şen, Z., Şişman, E., Kizilöz, B., 2022. A new innovative method for model efficiency performance. Water Supply 22, 589–601.
Sogut, E., Hsu, T.J., Farhadzadeh, A., 2022. Experimental and numerical investigations of solitary wave-induced non-equilibrium scour around structure of square cross-section on sandy berm. Coast. Eng. 173, 104091.
Soulsby, R., 1997. Dynamics of Marine Sands.
Soulsby, R.L., Whitehouse, R.J.S., 1997. Threshold of sediment motion in coastal environments. Pacific Coasts and Ports' 97: Proceedings of the 13th Australasian Coastal and Ocean Engineering Conference and the 6th Australasian Port and Harbour Conference 1, 145 others.
Sumer, B.M., Fredsøe, J., Christiansen, N., 1992. Scour around vertical pile in waves. J. Waterw. Port, Coast. Ocean Eng. 118 (1), 15–31.
Sumer, B., Christiansen, N., Fredsøe, J., 1993. Influence of cross section on wave scour around piles. J. Waterw. Port, Coast. Ocean Eng. 119, 477–495.
Sumer, B.M., Fredsøe, J., 2001. Scour around pile in combined waves and current. J. Hydraul. Eng. 127, 403–411.
Sumer, B.M., Fredsøe, J., 2002. Time scale of scour around a large vertical cylinder in waves. In: The Twelfth International Offshore and Polar Engineering Conference others.
Tafarojnoruz, A., Lauria, A., 2020. Large eddy simulation of the turbulent flow field around a submerged pile within a scour hole under current condition. Coast Eng. J. 62, 489–503.
Van Der Vorst, H.A., 1992. A fast and smoothly converging variant of Bi-CG for the solution of nonsymmetric linear systems. SIAM J. Sci. Stat. Comput. 13, 631–644.
van Rijn, L.V., 1984. Sediment Transport: Part II. Suspended Load Transport.
Velioglu Sogut, D., Sogut, E., Farhadzadeh, A., Hsu, T.-J., 2024. Non-equilibrium scour evolution around an emerged structure exposed to a transient wave. J. Mar. Sci. Eng. 12, 946.
Wilcox, D.C., 1994. Turbulence Modelling for CFD. DCW Industries Inc., La Canada. Cal., USA.
Willmott, C.J., 1981. On the validation of models. Phys. Geogr. 2, 184–194.
Yao, W., An, H., Draper, S., Cheng, L., Harris, J.M., 2018. Experimental investigation of local scour around submerged piles in steady current. Coast. Eng. 142, 27–41.
Zhao, M., Cheng, L., Zang, Z., 2010. Experimental and numerical investigation of local scour around a submerged vertical circular cylinder in steady currents. Coast. Eng. 57, 709–721.
Zhao, M., Zhu, X., Cheng, L., Teng, B., 2012. Experimental study of local scour around subsea caissons in steady currents. Coast. Eng. 60, 30–40.